The Tungsten–Tungsten Triple Bond. 17.[1] Mixed Amido–Phosphido Compounds of Formula $M_2(PR_2)_2(NMe_2)_4$. Comparisons of Amido and Phosphido Ligation and Bridged and Unbridged Isomers

William E. Buhro, Malcolm H. Chisholm,* Kirsten Folting, John C. Huffman, James D. Martin, and William E. Streib

Contribution from the Department of Chemistry and Molecular Structure Center, Indiana University, Bloomington, Indiana 47405. *Received April 26, 1991*

Abstract: The reaction between 1,2-$W_2Cl_2(NMe_2)_4$ and 2 equiv of a lithium organophosphide reagent, $LiPR_2$ (R = *t*-Bu, Cy, Et, $SiMe_3$, Ph, *p*-tol, *p*-C_6H_4F), in THF (tetrahydrofuran) at or below 0 °C yields the mixed amido–phosphido complexes 1,2-$W_2(PR_2)_2(NMe_2)_4$. The molybdenum analogue where R = *t*-Bu has been similarly prepared. With the sterically demanding *t*-Bu and $SiMe_3$ substituents at phosphorus, the products of a single substitution, 1,2-$W_2Cl(PR_2)(NMe_2)_4$, have been obtained. The latter react with a second equivalent of lithium organophosphide to yield the mixed-phosphido complexes 1,2-$W_2(PR_2)(PR'_2)(NMe_2)_4$. By single-crystal X-ray crystallography five samples have been fully characterized in the solid state. This structural data base contains both *anti*- and *gauche*-$M_2P_2N_4$ ethane-like cores with M–M distances typical of $(M{\equiv}M)^{6+}$ containing compounds with $\sigma^2\pi^4$ triple bonds: M–M = 2.2 (M = Mo) and 2.3 Å (M = W). The coordination about nitrogen is trigonal planar with short M–N distances, 1.96 Å (av), indicative of M–N double bonds, while the coordination at phosphorus is distinctly more pyramidal and the M–P distances of 2.42 to 2.48 Å are only slightly shorter than those anticipated for M–P single-bond distances. In solution, ^{31}P NMR chemical shifts, as well as the measured barriers to rotation about the M–N and M–P bonds, indicate a competition between metal–amido and metal–phosphido bonding that can be controlled by the substituents at phsophorus, e.g. $P(t\text{-Bu})_2$ is a better $\sigma + \pi$ donor than PPh_2. The measured rates of gauche:anti isomerization and the equilibrium constants are used to calculate thermodynamic and activation parameters for the rotation about the metal–metal bond. Except for bulky R groups, R = $SiMe_3$ and *t*-Bu, isomerization to phosphido-bridged dimers occurs in hydrocarbon solutions above 0 °C. The solid-state structure of $W_2(\mu\text{-}PCy_2)_2(NMe_2)_4$ deduced from an X-ray study reveals a central puckered W_2P_2 moiety with a dihedral angle between the W_2P planes of 130°. The M–M distance is 2.570 (1) Å, roughly 0.3 Å longer than in the unbridged isomer. The W–P distances, 2.36 (1) to 2.40 (1) Å, are equal or slightly shorter than those of the unbridged isomer while the W–N distances, 1.99 (1) Å (av), are notably longer. A MO analysis employing the Fenske–Hall method indicates that the puckered d^3–d^3 W_2P_2 moiety is favored relative to the planar $W_2(\mu\text{-}PR_2)_2$ moiety by enhanced M–M bonding. In solution two dynamic processes are observed: (i) rotation about M–N bonds and (ii) an inversion of the W_2P_2 moiety. The bridged isomers are characterized by lower field ^{31}P chemical shifts, ca. 180–280 ppm, and larger values of $J_{^{183}W\text{-}^{31}P}$ of ca. 250–350 Hz, relative to their unbridged isomers. The rate of bridge formation has been studied as a function of the substituents at phosphorus. Bridge formation (ring closure) shows first-order irreversible kinetics for R = Cy, Et and R = *t*-Bu and R′ = Ph and first-order reversible kinetics for R = Ph, *p*-tolyl, and *p*-C_6H_4F. Bridge formation is favored for the more Lewis basic phosphide ligands but suppressed by steric factors for the most bulky group R = *t*-Bu.

Introduction

The dinuclear unit $(M{\equiv}M)^{6+}$, where M = Mo and W, provides the template for an extensive chemistry.[2] Herein we describe the syntheses, structures, and solution behavior of mixed amido–phosphido compounds of the formula $W_2(PR_2)_2(NMe_2)_4$. This work provides the opportunity to compare (i) the bonding of amido and phosphido ligands to tungsten and (ii) the bonding in unbridged and bridged isomers. The bridged isomers $W_2(\mu\text{-}PR_2)_2(NMe_2)_4$ are a new structural type for d^3–d^3 dimers.[3] This work also provides the first observation of phosphido bridge opening and closing at a dinuclear center.[4] Preliminary communications have appeared.[5]

Results and Discussion

Synthesis. (a) Unbridged Isomers. The reaction between 1,2-$W_2Cl_2(NMe_2)_4$[6] and 2 equiv of a lithium phosphide, $LiPR_2$, in tetrahydrofuran at or below 0 °C yields a yellow solution of the ethane-like dimers, 1,2-$W_2(PR_2)_2(NMe_2)_4$ (R = *t*-Bu (**1**), Cy (**2**), Et (**3**), $SiMe_3$ (**4**), Ph (**5**), *p*-tol (**6**), and *p*-C_6H_4F (**7**), as described in eq 1. Upon extraction with hydrocarbon solvents, such as hexane or toluene, orange crystalline or microcrystalline

$$1,2\text{-}W_2Cl_2(NMe_2)_4 + 2LiPR_2 \xrightarrow{\leq 0\ ^\circ C} 1,2\text{-}W_2(PR_2)_2(NMe_2)_4 + 2LiCl \quad (1)$$

samples were isolated in 40–80% yields based on the tungsten starting material. The compound $Mo_2(P(t\text{-Bu})_2)_2(NMe_2)_4$ was prepared similarly.

With sterically demanding R groups, such as *t*-Bu and $SiMe_3$, bound to phosphorus, a single tungsten–chlorine substitution occurs when 1 equiv of lithium phosphide is added to a THF solution of 1,2-$W_2Cl_2(NMe_2)_4$ at less than −40 °C as described in eq 2. Upon extraction into hydrocarbon solvents the monophosphide

$$1,2\text{-}W_2Cl_2(NMe_2)_4 + LiPR_2 \xrightarrow{\leq -40\ ^\circ C} 1,2\text{-}W_2Cl(PR_2)(NMe_2)_4 + LiCl \quad (2)$$

complexes may be obtained as an oil for R = *t*-Bu (**8**) and as a crystalline product for R = $SiMe_3$ (**9**). The monophosphide complexes where R = Cy (**10**) and Ph (**11**) have been observed as minor components in reactions monitored by NMR. The chloride–phosphide complex **8** isomerizes in solution to the 1,1-

(1) (a) For Part 16 see: Chisholm, M. H.; Hampden-Smith, M. J.; Stahl, K. A.; Huffman, J. C.; Martin, J. D.; Moodley, K. G. *Polyhedron* **1988**, *7*, 1991. (b) This work is based in part on the Ph.D. Thesis of J. D. Martin, Indiana University, 1990.

(2) (a) Chisholm, M. H. *Acc. Chem. Res.* **1990**, *23*, 419. (b) Chisholm, M. H. *Angew. Chem., Int. Ed. Engl.* **1986**, *25*, 21.

(3) This structural type was first observed in the complex $W_2(PPh_2)_2(O\text{-}t\text{-Bu})_4$. Buhro, W. E.; Chisholm, M. H.; Folting, K.; Eichhorn, B. W.; Huffman, J. C. *J. Chem. Soc., Chem. Commun.* **1987**, 845.

(4) (a) Wojcicki, A. *Inorg. Chim. Acta* **1985**, *100*, 125. (b) Harley, A. D.; Whittle, R. R.; Geoffroy, G. L. *Organometallics* **1983**, *2*, 383.

(5) (a) Buhro, W. E.; Chisholm, M. H.; Folting, K.; Huffman, J. C. *J. Am. Chem. Soc.* **1987**, *109*, 905. (b) Buhro, W. E.; Chisholm, M. H.; Folting, K.; Huffman, J. C.; Martin, J. D.; Streib, W. E. *J. Am. Chem. Soc.* **1988**, *110*, 6563.

(6) Akiyama, M.; Chisholm, M. H.; Cotton, F. A.; Extine, M. W.; Murillo, C. A. *Inorg. Chem.* **1977**, *16*, 2407.

0002-7863/92/1514-557$03.00/0

$W_2Cl(PR_2)(NMe_2)_4$ isomer **18** upon standing for several days at room temperature.

The mixed phosphido complexes 1,2-$W_2(PR_2)(PR'_2)(NMe_2)_4$ (R = *t*-Bu, R' = Cy (**12**); R = *t*-Bu, R' = Ph (**13**); R = $SiMe_3$, R' = Cy (**14**); and R = $SiMe_3$, R' = Ph (**15**)), with different phosphido ligands bound to each metal, were prepared by reaction of a 1,2-$W_2Cl(PR_2)(NMe_2)_4$ complex with 1 equiv of a second lithium phosphide in THF solutions at −40 to 0 °C (eq 3). Crystals or microcrystalline powders of these materials were isolated by

$$1,2\text{-}W_2Cl(PR_2)(NMe_2)_4 + LiPR'_2 \rightarrow 1,2\text{-}W_2(PR_2)(PR'_2)(NMe_2)_4 + LiCl \quad (3)$$

recrystallization from hydrocarbon solvents. The complexes R = $SiMe_3$, R' = *t*-Bu (**16**) and R = $SiMe_3$, R' = Et (**17**) were identified by ^{31}P NMR spectroscopy but were not isolated.

(b) Bridged Isomers. Except for the complexes in which R = $SiMe_3$ and R = R' = $SiMe_3$ or *t*-Bu, the mixed amido–phosphido complexes react in solution above 0 °C to yield phosphido-bridged isomers, eq 4. Studies of the kinetics of reaction 4 are presented later in this paper.

$$1,2\text{-}W_2(PR_2)(PR'_2)(NMe_2)_4 \xrightarrow[\text{hydrocarbon}]{>0\ ^\circ C} W_2(\mu\text{-}PR_2)(\mu\text{-}PR'_2)(NMe_2)_4 \quad (4)$$

Since some compounds can be isolated in three forms, or at least detected in solution to exist in three forms, namely anti and gauche unbridged rotamers and the bridged isomer, we refer to each compound by a number and a letter, **a**, **g**, or **b**. Thus **2a**, **2b**, and **2g** refer to the anti, bridged, and gauche forms of $W_2(PCy_2)_2(NMe_2)_4$. In appearance the crystalline samples are yellow-orange for the anti rotamers, red-orange for the gauche rotamers, and dark brown for the bridged isomers. All are hydrocarbon soluble and air and moisture sensitive.

Solution Characterization. The amido–phosphido compounds are readily characterized by ^1H and ^{31}P NMR spectroscopy. Terminally bound phosphido ligands show coupling to ^{183}W, $I = {}^1/_2$, and 14.5% natural abundance while the bridged isomers show satellites of roughly twice the intensity reflecting the higher probability of adjacent ^{183}W and ^{31}P nuclides. The satellites due to coupling to two ^{183}W nuclei are not routinely observed, nor are two-bond ^{183}W–^{31}P interactions. For a given compound the chemical shifts fall in the order anti < gauche < bridged, i.e. the bridged are most deshielded. The chemical shifts of the bridged isomers are roughly 100 to 150 ppm downfield of the gauche and anti isomers consistent with the rehybridization of the phosphido ligand through bridge formation and the deshielding effect of the metal–metal bond.[7] Also worthy of note is that the $J_{^{183}W-^{31}P}$ values of the gauche rotamers are larger by roughly 50 Hz than those for the anti rotamers.

The ^1H NMR spectra are temperature dependent as will be described in detail later. However, the observed low-temperature spectra are consistent with the solid-state structures described below. The anti rotamer has one type of NMe_2 ligand, the gauche rotamer has two types, and at low temperatures the bridged isomer also has two types. The compounds of formula $W_2(PR_2)(PR'_2)(NMe_2)_4$ and $W_2Cl(PR_2)(NMe_2)_4$ that exist in unbridged forms as both anti and gauche rotamers contain two different tungsten atoms. Thus for the anti rotamer there are two types of NMe_2 ligands and there are four for the gauche. ^{31}P–^{31}P coupling was not generally observed but was seen for the compound **12** (R = Cy, R' = *t*-Bu) with a value of 6 Hz. Presumably in the other compounds where R ≠ R' this coupling constant is small.

A summary of ^1H and ^{31}P NMR data is given in Table I.

Solid-State Molecular Structures. (a) Unbridged Isomers. Five examples of these mixed phosphido–amido ditungsten compounds have been characterized by X-ray diffraction studies, together with one molybdenum analogue *anti*-$Mo_2(P(t\text{-}Bu)_2)_2(NMe_2)_4$. A summary of crystal data is given in Table II.

(7) *Phosphorus-31 NMR Spectroscopy in Stereochemical Analysis: Organic Compounds and Metal Complexes*; Verkade, J. G., Quin, L. D., Eds.; VCH Publishers: Deerfield Beach, FL, 1987.

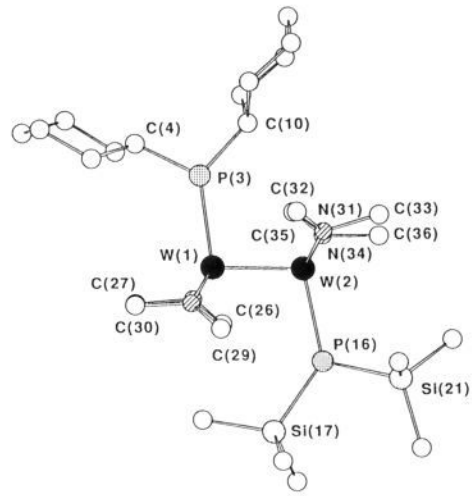

Figure 1. Ball-and-stick drawing of the *anti*-1,2-$W_2(P(SiMe_3)_2(PCy_2)(NMe_2)_4$ molecule giving the atom numbering scheme.

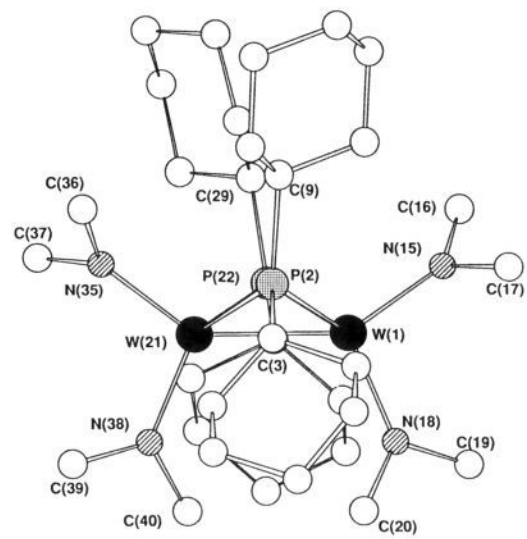

Figure 2. Ball-and-stick drawing of the $W_2(\mu\text{-}PCy_2)_2(NMe_2)_4$ molecule giving the atom numbering scheme.

A ball-and-stick drawing of the mixed phosphido molecule $W_2(PCy_2)(P(SiMe_3)_2)(NMe_2)_4$ is shown in Figure 1. It shows the now familiar ethane-like core with the anti conformation for a 1,2-disubstituted compound. The methyl groups of the NMe_2 ligands are aligned along the M–M axis as are the substituents at phosphorus. The appearance of a gauche rotamer can easily be anticipated on the basis of Figure 1. A summary of the pertinent structural parameters is given in Table III. In the case of *anti*-$W_2(P(SiMe_3)_2)_2(NMe_2)_4$, there were two independent molecules in the unit cell. The observed structural differences between these two forms of the same compound serve to indicate how crystal packing may influence the various structural parameters. With the exception of the sum of the angles at phosphorus, these differences are within 3σ.

The M–M distances are within the range expected for triple bonds of configuration $\sigma^2\pi^4$ in ethane-like dinuclear compounds.[2] The M–N distances fall within a very narrow range, 1.95–1.97 Å, typical of what we have previously suggested to be equivalent to a double bond, $\sigma^2\pi^2$.[8] Coordination about nitrogen is trigonal planar. The M–P distances span a slightly larger range, 2.40–2.48

(8) (a) Chisholm, M. H.; Cotton, F. A.; Extine, M. W.; Stults, B. R. *J. Am. Chem. Soc.* **1976**, *98*, 4477. (b) Chisholm, M. H.; Cotton, F. A.; Frenz, B. A.; Shive, L. W.; Stults, B. R. *J. Am. Chem. Soc.* **1976**, *98*, 4469. (c) Chisholm, M. H.; Cotton, F. A.; Extine, M. W.; Millar, M.; Stults, B. R. *Inorg. Chem.* **1976**, *15*, 2244.

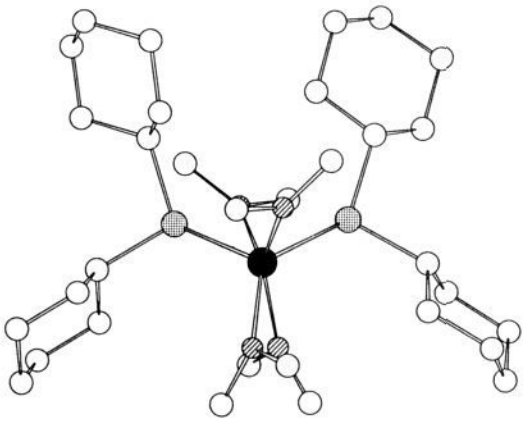

Figure 3. View of the $W_2(\mu\text{-}PCy_2)_2(NMe_2)_4$ molecule looking down the metal–metal vector, emphasizing the puckered nature of the W_2P_2 core.

Å, and the angles at phosphorus are distinctly pyramidal. However, the latter must be easily deformable since for *anti*-$W_2(P(SiMe_3)_2)_2(NMe_2)_4$ the angles are 345° and 352° for the two independent molecules in the unit cell.

(b) Bridged Isomer. Two views of the solid-state molecular structure of $W_2(\mu\text{-}PCy_2)_2(NMe_2)_4$ (**2b**) are shown in Figures 2 and 3, and a listing of selected bond distances and angles is given in Table IV. The structure may be viewed as being derived from an edge-shared bitetrahedron with a central puckered W_2P_2 core. The distortion renders the two terminal NMe_2 groups inequivalent. The angle between the two W_2P planes is 129.6°. The W–W distance of 2.5701 (6) Å is almost 0.3 Å longer than that in the unbridged isomer **2g** though the W–P distances 2.35–2.40 Å are essentially the same or slightly shorter than those in **2g**. The M–N distances on the other hand are slightly longer, 1.97–2.00 Å. The coordination at nitrogen is trigonal planar, but the NC_2 units are not aligned directly along the M–M axis as in the unbridged isomer.

Dynamic NMR Studies. (a) Rotations about M–N, M–P, and M–M Bonds. As with other 1,2-$W_2X_2(NMe_2)_4$ complexes,[8] rotations about M–N bonds may be monitored by VT NMR spectroscopy. From the low-temperature-limiting spectra and the coalescence temperatures we have calculated the free energy of activation, $\Delta G^{\ddagger}_{rot}(T_c)$. Similar behavior is observed and calculations have been performed for rotations about the M–P bonds. These data are summarized in Table V. The significance of these $\Delta G^{\ddagger}_{rot}(T_c)$ values, in terms of metal ligand π bonding, will be discussed later in this paper.

Though the M–M triple bond in ethane-like dimers is cylindrical, the cogging effect of the NC_2 and PC_2 units imposes a significant barrier to anti ⇄ gauche isomerization and this is not rapid on the NMR time scale. However, starting with a pure anti or pure gauche crystalline sample, we have monitored the approach to equilibrium as a function of time, temperature, and substituent R. Ground-state and activation parameters were determined from plots of ln $(K_{eq}/2)$ vs $1/T$ and Eyring plots, respectively. Data are presented in Table VI.

Very-small ground-state differences are observed between the anti and gauche rotamers as is necessary for both species to be present in nearly equal concentrations at equilibrium. Both the substituents at phosphorus and the metal (M = Mo vs W) have control over the thermodynamic preference in ways that we do not yet understand. There is no obvious steric or electronic dominance. For example, it could be reasoned that the complex $W_2(P(SiMe_3)_2)_2(NMe_2)_4$ favors >90% the anti rotamer because of the large steric demand of the phosphido ligands. However, the even bulkier $P(t\text{-}Bu)_2$ complex favors the gauche over the anti by 4:1 and the less sterically demanding PPh_2 complex favors the anti by 6:1.

The activation parameters for anti ⇄ gauche isomerization are similar to those seen for related 1,2-$M_2X_2(NR_2)_4$ compounds.[8] The negative entropy of activation of ca. −10 eu is suggestive of some degree of ordering in the transition state and probably reflects the decogging of the NC_2 and PC_2 blades.

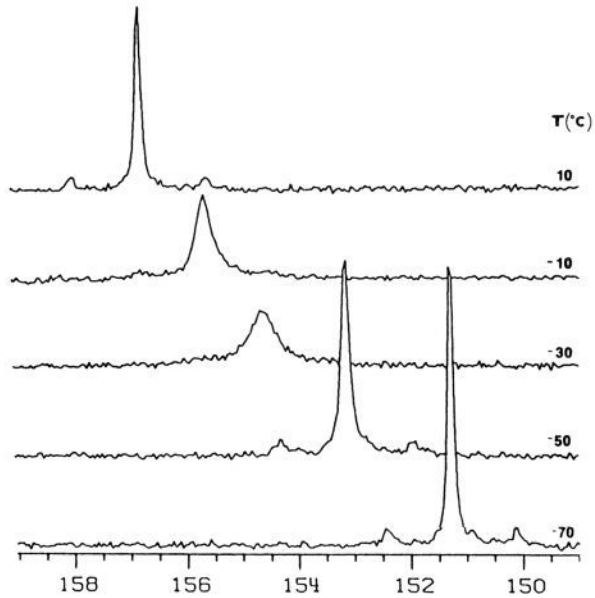

Figure 4. Variable-temperature $^{31}P\{^1H\}$ spectra of a toluene-d_8 solution of *gauche*-1,2-$W_2(PCy_2)_2(NMe_2)_4$ (**2g**). The chemical shift scale is reported in δ (ppm).

(b) Inversion of the W_2P_2 Moeity in $W_2(\mu\text{-}PCy_2)_2(NMe_2)_4$. The low-temperature-limiting ^1H NMR spectrum (−80 °C) of $W_2(\mu\text{-}PCy_2)_2(NMe_2)_4$ shows two types of NMe_2 ligands in the ratio 1:1. One of the NMe_2 ligands is undergoing slow proximal and distal exchange of its NMe groups while the other is still rapid on the NMR time scale. In addition there are signals due to two cyclohexyl α-hydrogens which are readily distinguished from the other broad and overlapping cyclohexyl resonances. Upon raising the temperature the signals associated with the α-cyclohexyl hydrogen atoms coalesce into the base line and then sharpen at room temperature. A similar behavior is observed for the NMe groups such that rotations about the M–N bonds are rapid and there is only one type of NMe_2 ligand. This behavior is consistent with the maintenance of the puckered W_2P_2 structure in solution at low temperature but indicates that there is inversion on the NMR time scale at room temperature. To the extent that the central W_2P_2 unit may be called a butterfly (or opened tetrahedron) we observe the butterfly flapping its wings. This inversion or wing flapping causes the two NMe_2 groups to become equivalent. Schematically this dynamic process is shown in I below. The transition state is the symmetrical edge-shared bitetrahedral structure.

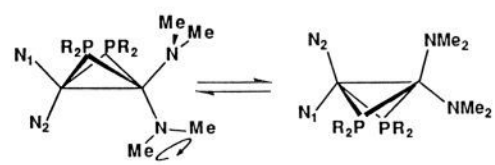

I

The barrier to wing flapping or inversion can be calculated from either the α-cyclohexyl proton coalescence or the coalescence of the NMe_2 groups. The $\Delta G^{\ddagger}(T_c)$ values are listed in Table VII along with some data for the related compounds of formula $W_2(\mu\text{-}PR_2)_2(O\text{-}t\text{-}Bu)_4$.

(c) Temperature Effects on ^{31}P Chemical Shifts and ^{183}W–^{31}P Coupling Constants. On lowering the temperature from 22 to −80 °C the unbridged isomers show a consistent chemical shift drift to higher field and a parallel decrease in the magnitude of $^1J_{^{183}W-^{31}P}$. These changes are illustrated by the data shown in Table VIII. In addition, for the compounds *gauche*-$W_2(PCy_2)_2(NMe_2)_4$, *anti*-$W_2(PCy_2)(P(SiMe_3)_2(NMe_2)_4$, and *gauche*-$W_2Cl(P(SiMe_3)_2)(NMe_2)_4$ there are line-shape changes with temperature

Table I. NMR and IR Characterization of Complexes **1–18**

complex	^{31}P δ; J_{WP}, Hz; I, %	^{1}H NMR
anti-1,2-$Mo_2(P(t\text{-}Bu)_2)_2(NMe_2)_4$	196.2 (s)[a]	3.51 (d, $^4J_{HP}$ = 2.3 Hz, 24 H), 1.46 (d, $^3J_{HP}$ = 12.4 Hz, 36 H)[b]
gauche-1,2-$Mo_2(P(t\text{-}Bu)_2)_2(NMe_2)_4$	216.2 (s)[a]	3.68–3.45 (br s, 12 H), 3.47 (d, $^4J_{HP}$ = 2.5 Hz, 12 H), 1.53 (d, $^3J_{HP}$ = 12.4 Hz, 36 H)[b]
anti-1,2-$W_2(P(t\text{-}Bu)_2)_2(NMe_2)_4$ (**1a**)	178.2; 285.6; 14	3.47 (d, $^4J_{HP}$ = 1.4 Hz, 24 H), 1.50 (d, $^3J_{HP}$ = 12.4 Hz, 36 H)[b]
gauche-1,2-$W_2(P(t\text{-}Bu)_2)_2(NMe_2)_4$ (**1g**)	199.7; 333.0; 15	3.58–3.45 (br s, 12 H), 3.42 (d, $^4J_{HP}$ = 1.62 Hz), 1.56 (d, $^3J_{HP}$ = 12.9 Hz, 36 H)[b]
anti-1,2-$W_2(PCy_2)_2(NMe_2)_4$ (**2a**)	133.7; 312; 15	3.48 (s, 24 H)[b,d]
$W_2(\mu\text{-}PCy_2)_2(NMe_2)_4$ (**2b**)	228.4; 305; 24	3.43 (s, 24 H), 2.21 (m, 4 H), 1.91 (m, 8 H), 1.70 (m, 4 H)[a,c]
gauche-1,2-$W_2(PCy_2)_2(NMe_2)_4$ (**2g**)	156.5; 341.0; 15	3.43 (s, 12 H), 3.41 (s, 12 H), 2.87–2.68 (br s, 4 H), 2.48–2.30 (br m, 8 H), 1.95–1.77 (br m, 8 H), 1.68 (br d, J = 12.5 Hz, 4 H), 1.61–1.12 (br m, 20 H)[b]
anti-1,2-$W_2(PEt_2)_2(NMe_2)_4$ (**3a**)	70.7; 230; 14	3.31 (br s, 24 H), 2.40 (m, 8 H), 1.36 (d of t, $^3J_{HH}$ = 7.44 Hz, $^3J_{HP}$ = 13.5 Hz, 12 H)[b]
$W_2(\mu\text{-}PEt_2)_2(NMe_2)_4$ (**3b**)	195.3; 319; 25 (0 °C)	3.38 (s, 24 H), 2.52 (br, 8 H), 1.15 (d of t, $^3J_{HH}$ = 7.6 Hz, $^3J_{HP}$ = 16.6 Hz, 12 H)[b]
gauche-1,2-$W_2(PEt_2)_2(NMe_2)_4$ (**3g**)	91.1; 220; 14	3.29 (s, 12 H), 3.25 (s, 12 H), 1.45 (m, 12 H)[b,d]
anti-1,2-$W_2(P(SiMe_3)_2)_2(NMe_2)_4$ (**4a**)	−106.7; 243; 14	3.48–3.30 (br s, 24 H), 0.45 (d, $^3J_{HP}$ = 4.7 Hz, 36 H)[a]
gauche-1,2-$W_2(P(SiMe_3)_2)_2(NMe_2)_4$ (**4g**)	−88.3; 250; 14	0.54 (d, $^3J_{HP}$ = 4.7 Hz, 36 H)[a,d]
anti-1,2-$W_2(PPh_2)_2(NMe_2)_4$ (**5a**)	61.8; 207; 15	7.71 (d of d, $^3J_{HP}$ = 8.1 Hz, $^3J_{HH}$ = 8.4 Hz, 8 H), 7.07 (d of d, $^3J_{HH}$ = 7.8 Hz, $^3J_{HH}$ = 6.0 Hz, 8 H), 6.96 (t, $^3J_{HH}$ = 7.2 Hz, 4 H), 3.25–2.80 (br s, 24 H)[a]
$W_2(\mu\text{-}PPh_2)_2(NMe_2)_4$ (**5b**)	186.5; 334; 24	7.58 (d of d, $^3J_{HP}$ = 10.1 Hz, $^3J_{HH}$ = 8.3 Hz, 8 H), 7.22 (d of d, $^3J_{HH}$ = 7.0 Hz, $^3J_{HH}$ = 7.1 Hz, 8 H), 7.04 (t, $^3J_{PH}$ = 7.6 Hz, 4 H), 3.22 (s, 24 H)[a]
gauche-1,2-$W_2(PPh_2)_2(NMe_2)_4$ (**5g**)	88.4; 263; 15	7.98 (d of d, $^3J_{HP}$ = 8.4 Hz, $^3J_{HH}$ = 8.4 Hz, 8 H), 3.22 (s, 12 H), 3.15–3.05 (br s, 12 H)[a,d]
anti-1,2-$W_2(P(p\text{-}tol)_2)_2(NMe_2)_4$ (**6a**)	63.3; 214; 16	7.68 (d of d, $^3J_{HP}$ = 8.4 Hz, $^3J_{HH}$ = 8.4 Hz, 8 H), 6.95 (d, $^3J_{HH}$ = 8.2 Hz), 3.17 (br s, 24 H), 2.12 (s, 12 H)[a]
$W_2(\mu\text{-}P(p\text{-}tol)_2)_2(NMe_2)_4$ (**6b**)	185.4; 331; 24	7.57 (d of d, $^3J_{PH}$ = 10.5 Hz, $^3J_{HH}$ = 7.7 Hz, 8 H), 7.10 (d, $^3J_{HH}$ = 7.5 Hz, 8 H), 3.28 (s, 24 H), 2.14 (s, 12 H)[a]
gauche-1,2-$W_2(P(p\text{-}tol)_2)_2(NMe_2)_4$ (**6g**)	91.3; 282; 14	7.94 (d of d, $^3J_{HP}$ = 8.6 Hz, $^3J_{HH}$ = 8.0 Hz, 8 H), 7.03 (d, $^3J_{HH}$ = 7.5 Hz, 8 H), 3.22 (s, 12 H), 2.10 (s, 12 H)[a,d]
anti-1,2-$W_2(P(p\text{-}FPh)_2)_2(NMe_2)_4$ (**7a**)	57.4; 208; 16	7.38 (d of d of d, $^3J_{HP}$ = 8.2 Hz, $^3J_{HH}$ = 8.2 Hz, $^4J_{HF}$ = 5.5 Hz, 8 H), 6.72 (d of d, $^3J_{HH}$ = 8.5 Hz, $^3J_{HF}$ = 8.5 Hz, 8 H), 2.9 (br s, 24 H)[b]
$W_2(\mu\text{-}P(p\text{-}FPh)_2)_2(NMe_2)_4$ (**7b**)	182.9; 339; 26	7.28 (d of d of d, $^3J_{HP}$ = 8 H), 6.85 (d of d, 8 H), 3.13 (s, 24 H)[a]
gauche-1,2-$W_2(P(p\text{-}FPh)_2)_2(NMe_2)_4$ (7g)	79.4; 256; 15	7.62 (d of d of d, $^3J_{HP}$ = 8 H), 6.80 (d of d, 8 H), 3.04 (s, 12 H)[b,d]
anti-1,2-$W_2Cl(P(t\text{-}Bu)_2)(NMe_2)_4$ (**8a**)	151.7; 200; 14	
gauche-1,2-$W_2Cl(P(t\text{-}Bu)_2)(NMe_2)_4$ (**8g**)	172.6; 233.5; 16	4.52 (v br s, 3 H), 4.07 (br s, 3 H), 3.46 (s, 6 H), 3.27 (s, 6 H), 2.44 (br s, 3 H), 2.40 (v br s, 3 H), 1.62 (d, $^3J_{HP}$ = 12.5 Hz, 18 H)[a]
anti-1,2-$W_2Cl(P(SiMe_3)_2)(NMe_2)_4$ (**9a**)	−100.3; 228; 14	4.36 (s, 6 H), 3.37 (s, 12 H), 2.40 (s, 6 H), 0.41 (d, $^4J_{HP}$ = 5.4 Hz, 18 H)[a]
gauche-1,2-$W_2Cl(P(SiMe_3)_2)(NMe_2)_4$ (**9g**)	−89.0; 243; 15	4.08 (s, 3 H), 3.3 (br s, 6 H), 3.2 (br s, 6 H), 2.48 (s, 3 H), 2.2 (br s, 3 H), 0.56 (d, $^3J_{PH}$ = 4.8 Hz, 36 H)[a,d]
gauche-1,2-$W_2Cl(PCy_2)(NMe_2)_4$ (**10g**)	146.7	
anti-1,2-$W_2Cl(PPh_2)(NMe_2)_4$ (**11a**)	56.1; 213; 14	
gauche-1,2-$W_2Cl(PPh_2)(NMe_2)_4$ (**11g**)	72.4; 235; 15	
anti-1,2-$W_2(P(t\text{-}Bu)_2)(PCy_2)(NMe_2)_4$ (**12a**)	186.5; 308; 15 129.0; 289.2; 14	3.52 (d, $^4J_{HP}$ = 1.6 Hz, 12 H), 3.41 (s, 12 H), 2.52–2.38 (m, 2 H), 2.30 (br d, J = 13.2 Hz, 4 H), 1.83 (br d, J = 12.6 Hz, 2 H) 1.69 (br d, J = 12.7 Hz, 2 H), 1.6–1.1 (br m, 10 H), 1.52 (d, $^3J_{HP}$ = 12.7 Hz, 18 H)[b]
$W_2(\mu\text{-}P(t\text{-}Bu)_2)(\mu\text{-}PCy_2)(NMe_2)_4$ (**12b**)	272.4; 269; 9.5; 24 228.6; 313; 24	3.38 (s, 24 H), 1.42 (d, $^3J_{HP}$ = 12.7 Hz, 18 H)[a,c]
gauche-1,2-$W_2(P(t\text{-}Bu)_2)(PCy_2)(NMe_2)_4$ (**12g**)	188.4; 311.4; 16 160.5; 360; 16	3.53 (s, 6 H), 3.48 (d, $^4J_{HP}$ = 1.9 Hz, 6 H), 3.36 (d, $^4J_{HP}$ = 1.2 Hz, 6 H), 3.34 (br s, 6 H), 2.91–2.76 (br m, 2 H), 2.50–2.35 (br m, 4 H) 1.91–1.78 (br m, 4 H), 1.68 (br d, J = 12 Hz, 2 H),[c] 1.7–1.1 (br m, 10 H), 1.57 (d, $^3J_{HP}$ = 12.7 Hz, 18 H)[b]
anti-1,2-$W_2(P(t\text{-}Bu)_2(PPh_2)(NMe_2)_4$ (**13a**)	185.9; 294; 15 61.3; 205; 14	7.78 (d of d, $^3J_{PH}$ = 8.1 Hz, $^3J_{HH}$ = 8.2 Hz, 4 H), 3.44 (s, 12 H), 3.07 (s, 12 H), 1.47 (d, $^3J_{PH}$ = 13 Hz, 18 H)[b,d]
$W_2(\mu\text{-}P(t\text{-}Bu)_2)(\mu\text{-}PPh_2)(NMe_2)_4$ (**13b**)	257.1; 257; 25 189.2; 364.7; 26	7.48 (d of d, $^3J_{HP}$ = 10 Hz, $^3J_{HH}$ = 8.4 Hz, 4 H), 7.13 (d of d, $^3J_{HH}$ = 8.1 Hz, 4 H), 3.36 (br s, 24 H) 1.40 (d, $^3J_{HP}$ = 13 Hz, 18 H)[a,c]
gauche-1,2-$W_2(P(t\text{-}Bu)_2)(PPh_2)(NMe_2)_4$ (**13g**)	203.3; 315; 15 91.7; 269; 15	7.97 (d of d, $^3J_{PH}$ = 8.3 Hz, $^3J_{HH}$ = 8.3 Hz, 4 H), 3.48 (s, 6 H), 3.46 (s, 6 H), 1.55 (d, $^3J_{PH}$ = 13 Hz, 18 H)[b,d]
anti-1,2-$W_2(P(SiMe_3)_2)(PCy_2)(NMe_2)_4$ (**14a**)	134.2; 311; 14 −106.9; 239; 14	3.60–3.20 (br s, 12 H), 3.36 (s, 12 H), 0.47 (d, $^4J_{PH}$ = 5.1 Hz, 18 H)[a,d]
gauche-1,2-$W_2(P(SiMe_3)_2)(PCy_2)(NMe_2)_4$ (**14g**)	166.3; 390; 14 −96.3; 234; 14	0.53 (d, $^4J_{PH}$ = 4.7 Hz, 18 H)[a,d]
anti-1,2-$W_2(P(SiMe_3)_2)(PPh_2)(NMe_2)_4$ (**15a**)	107.9; 229; 14 63.9; 220; 14	7.75 (d of d, $^3J_{HP}$ = 4.9 Hz, $^3J_{HH}$ = 7.9 Hz, 4 H). 7.10 (d of d, $^3J_{HH}$ = 6.9 Hz, $^3J_{HH}$ = 7.6 Hz, 4 H), 6.98 (d, $^3J_{HH}$ = 7.6 Hz, 2 H), 3.35 (br s, 12 H) 3.30–2.95 (br s, 12 H), 0.43 (d, $^3J_{HP}$ = 4.7 Hz, 18 H)[a]
gauche-1,2-$W_2(P(SiMe_3)_2)(PPh_2)(NMe_2)_4$ (**15g**)	−84.4; 229 82.9; 269; 14	7.93 (d of d, $^3J_{HP}$ = 8.3 Hz, $^3J_{HH}$ = 8.3 Hz, 4 H), 6.96 (d, $^3J_{HH}$ = 7.2 Hz, 2 H)[a,d]
anti-1,2-$W_2(P(SiMe_3)_2)(P(t\text{-}Bu)_2)(NMe_2)_4$ (**16a**)	−114.1; 237; 14 179.9; 302; 14	
gauche-1,2-$W_2(P(SiMe_3)_2)(P(t\text{-}Bu)_2)(NMe_2)_4$ (**16g**)	−93.8; 234; 14 191.6; 327; 14	
anti-1,2-$W_2(P(SiMe_3)_2)(PEt_2)(NMe_2)_4$ (**17a**)	−112.5; 239; 14 63.3; 220; 14	
gauche-1,2-$W_2(P(SiMe_3)_2)(PEt_2)_2(NMe_2)_4$ (**17g**)	−89.8 82.2	
1,1-$W_2Cl(P(t\text{-}Bu)_2)(NMe_2)_4$ (**18**)	257.8; 411.6; 22.1; 14	4.38 (s, 3 H), 4.10 (v br s, 3 H), 3.40 (v br s, 6 H), 3.31 (s, 6 H), 2.84 (s, 3 H), 2.35 (v br s, 3 H), 1.71 (d, $^3J_{HP}$ = 13.6 Hz, 9 H), 1.22 (d, $^3J_{HP}$ = 12.3 Hz, 9 H)[a]

[a] In C_6D_6. [b] In $C_6D_5CD_3$. [c] In THF-d_8. [d] Incomplete listing; other resonances obscured or undetected. [e] Less than 0 °C.

Table II. Summary of Crystal Data

empirical formula	$C_{24}H_{60}Mo_2N_4P_2$	$C_{24}H_{60}N_4P_2W_2$	$C_{24}H_{60}N_4P_2W_2$	$C_{32}H_{68}N_4P_2W_2$	$C_{20}H_{60}N_4P_2Si_4W_2$	$C_{26}H_{64}N_4P_2Si_2W_2$
color of crystal	red	yellow	orange-yellow	orange	yellow	yellow-brown
crystal dimens (mm)	0.30 × 0.30 × 0.30	0.1 × 0.1 × 0.1	0.12 × 0.12 × 0.20	0.15 × 0.15 × 0.10	0.08 × 0.12 × 0.16	0.15 × 0.25 × 0.30
space group	$P2_1/n$	$P2_1/n$	$P2_1/n$	*Pnna*	*P*1	$P2_1/n$
temp (°C)	−156	−158	−155	−156	−157	−145
cell dimens						
a (Å)	9.763 (1)	10.364 (2)	12.225 (2)	23.249 (15)	11.941 (2)	10.594 (2)
b (Å)	18.210 (3)	10.489 (2)	18.250 (5)	15.979 (9)	14.751 (3)	12.850 (2)
c (Å)	10.031 (1)	14.559 (3)	14.666 (3)	10.119 (4)	10.303 (2)	27.348 (5)
α (deg)					92.15 (1)	
β (deg)	117.64 (0)	91.84 (1)	92.03 (1)		90.49 (1)	91.32 (1)
γ (deg)					89.07 (1)	
Z (molecules/cell)	2	2	4	4	2	4
vol (Å^3)	1579.68	1581.89	3269.92	3759.28	1813.17	3722.14
calcd density (g/cm^3)	1.385	1.752	1.695	1.658	1.646	1.639
wavelength (Å)	0.71069	0.71069	0.71069	0.71069		
mol wt	658.59	834.41	834.41	938.56	898.71	918.64
linear abs coeff (cm^{-1})	8.928	75.412	72.964	63.564	67.090	64.780
detector to sample dist (cm)	22.5	22.5	22.5	22.5	22.5	22.5
sample to source dist (cm)	23.5	23.5	23.5	23.5	23.5	23.5
av ω scan width at half height	0.25	0.25	0.25	0.25	0.25	0.25
scan speed (deg/min)	5.0	4.0	4.0	4.0	6.0	6.0
scan width (deg + dispersion)	1.8	1.8	2.0	1.6	1.8	1.5
individual bkgd (s)	6	8	6	8	6	6
aperture size (mm)	3.0 × 4.0	2.0 × 4.0	3.0 × 4.0	3.0 × 4.0	3.0 × 4.0	3.0 × 4.0
2θ range (deg)	6–50	6–45	6–45	6–45	5–55	6–45
total no. of reflcns collected	3558	4492	4535	2877	9352	5707
no. of unique intensities	2787	2071	4300	2475	8373	4876
no. with $F > 0.0$	2664			2106	7513	4383
no. with $F > 3.0\sigma(F)$	2525	1879	3810	1710	6808	3914
$R(F)$	0.0239	0.0182	0.0367	0.0668	0.0567	0.0660
$R_w(F)$	0.0274	0.0196	0.0381	0.0600	0.0540	0.0644
goodness of fit for the last cycle	0.804	0.710	0.969	1.100	1.787	1.768
max δ/σ for last cycle	0.05	0.05	0.05	0.05	0.08	1.50

Table III. Selected Structural Data for 1,2-$M_2(PR_2)_2(NMe_2)_4$ Compounds[a]

parameter	M = Mo, R = *t*-Bu	**1a**	**1g**	**2g**	**4a′**	**4a″**	**14a**
M–M	2.2137 (5)	2.3091 (5)	2.3200 (7)	2.294 (2)	2.2989 (9)	2.3025 (9)	2.3016 (10)
M–M (av)	1.976 (8)	1.965 (6)	1.97 (1)	1.97 (2)	1.963 (9)	1.956 (9)	1.848 (14) 1.939 (14)
M–P	2.477 (1)	2.470 (2)	2.398 (2)	2.401 (6)	2.423 (3)	2.444 (3)	2.368 (4) 2.425 (4)
Δ^b	0.50 (1)	0.50 (1)	0.43 (1)	0.43 (3)	0.46	0.49	0.419 0.486
sum of ∠P's[c]	348.6 (3)	346.0 (6)	355.5 (16)	347.0 (21)	352.5 (2)	345.0 (2)	351.1 (6) 348.5 (2)
M–M–N(av)	103.3 (1)	103.6 (1)	102.5 (25)	103.4 (12)	103.7 (3)	104.3 (3)	105.3 (5) 105.2 (4)
M–M–P	104.5 (1)	105.3 (1)	107.6 (3)	99.9 (1)	102.8 (1)	104.9 (1)	97.94 (11) 101.98 (10)
M–N–C(a)[d] (av)	133.0 (4)	132.8 (5)	132.4 (5)	134.2 (14)	134.2 (7)	133.6 (8)	134.3 (13) 134.0 (14)
M–N–C(b)[d] (av)	118.0 (7)	118.0 (6)	118.4 (9)	115.9 (14)	115.0 (7)	116.5 (7)	116.1 (11) 116.1 (12)
C(a)–N–C(b) (av)	108.8 (2)	109.0 (4)	109.0 (10)	109.7 (18)	110.8 (9)	109.7 (1)	109.4 (14) 108.8 (15)
M–P–C(a) [Si]	131.4 (1)	130.0 (2)	135.0 (3)	124.5 (6)	132.6 (2)	130.9 (1)	120.3 (6) 132.27 (22)
M–P–C(b) [Si]	109.2 (1)	108.2 (2)	111.9 (8)	116.7 (6)	113.2 (1)	109.9 (1)	127.1 (5) 109.72 (22)
C(a)–P–C(b) [Si–P–Si]	108.0 (1)	107.8 (2)	108.6 (5)	105.8 (9)	106.7 (2)	104.2 (2)	103.7 (7) 106.50 (24)

[a] Distances in angstroms and angles in degrees. [b] $\Delta = d(M–P) - d(M–N)$, the difference in M–P and M–N distances. [c] Sum of the bond angles about phosphorus. [d] a = proximal and b = distal.

as shown in Figure 4. We suggest that all these effects are related to inversion at phosphorus and that the coalescence type behavior (Figure 4) reflects the equilibration of invertamers having unequal distributions.[9]

(d) Studies of Bridge Formation. The compounds 1,2-$W_2(PR_2)_2(NMe_2)_4$, where R = *t*-Bu and $SiMe_3$, are inert with respect to bridge formation, and mixed phosphido compounds of the formula 1,2-$W_2(PR_2)(PR'_2)(NMe_2)_4$ are similarly inert when one of the groups R or R′ = $SiMe_3$. For other compounds we have monitored the rate of bridge formation by ^{31}P NMR spectroscopy in order to gain some insight into this process. Rate data obtained for several of the compounds at various temperatures are given in the thesis.[1b]

The bridge closure for the bis(dicyclohexylphosphido) complex **2** shows an irreversible first-order reaction as is evident from the

(9) Chisholm, M. H.; Huffman, J. C.; Pasterczyk, J. W. *Inorg. Chem.* **1987**, *26*, 3781.

Table IV. Selected Bond Distances (Å) and Angles (deg) for $W_2(\mu\text{-}PCy_2)_2(NMe_2)_4$ (**2b**)

A	B	distance
W(1)	W(21)	2.5701 (8)
W(1)	P(2)	2.359 (3)
W(1)	P(22)	2.405 (3)
W(1)	N(15)	2.004 (10)
W(21)	N(18)	1.983 (10)
W(21)	P(2)	2.393 (3)
W(21)	P(22)	2.354 (3)
W(21)	N(35)	1.996 (10)
W(21)	N(38)	1.972 (10)
P	C	1.88 (av)
N	C	1.46 (av)

A	B	C	angle
W(21)	W(1)	P(2)	57.89 (8)
W(21)	W(1)	P(22)	56.36 (8)
W(21)	W(1)	N(15)	142.8 (3)
W(21)	W(1)	N(18)	112.0 (3)
P(2)	W(1)	P(22)	98.94 (11)
P(2)	W(1)	N(15)	113.5 (3)
P(2)	W(1)	N(18)	115.1 (3)
P(22)	W(1)	N(15)	94.0 (3)
P(22)	W(1)	N(18)	129.5 (3)
N(15)	W(1)	N(18)	104.2 (4)
W(1)	W(21)	P(2)	56.63 (8)
W(1)	W(21)	P(22)	58.28 (8)
W(1)	W(21)	N(35)	139.6 (3)
W(1)	W(21)	N(38)	113.58 (27)
P(2)	W(21)	P(22)	99.44 (11)
P(2)	W(21)	N(35)	92.1 (3)
P(2)	W(21)	N(38)	130.2 (3)
P(22)	W(21)	N(35)	110.4 (3)
P(22)	W(21)	N(38)	115.6 (3)
N(35)	W(21)	N(38)	106.1 (4)
W(1)	P(2)	W(21)	65.48 (8)

linear plot of $-\ln [A]/[A_0]$ with time. See Figure 5. Rather interestingly, the bis(arylphosphido) complexes show reversible first-order kinetics for bridge closure as is evident from the linear plot of $-\ln [A - A_e]/[A_0 - A_e]$ with time. See Figure 6. At equilibrium the bridged isomer is favored over the ethane-like isomer by roughly 5:1 when R = Ph.

Mixed phosphido compounds of formula $1,2\text{-}W_2(PR_2)(PR'_2)(NMe_2)_4$ were also studied with regard to bridge formation and revealed some additional insight. For example, where R = *t*-Bu and R′ = Ph, bridge formation is complete and irreversible. When R = *t*-Bu and R′ = Cy, bridge formation is incomplete and

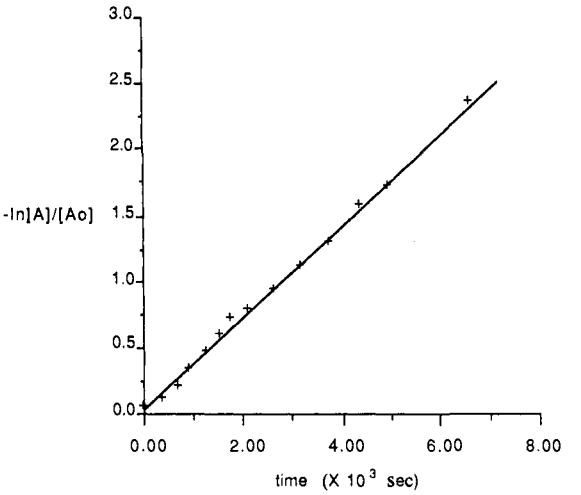

Figure 5. A plot of $-\ln [A]/[A_0]$ vs time demonstrating the irreversible first-order isomerization of $1,2\text{-}W_2(PCy_2)_2(NMe_2)_4$ to $W_2(\mu\text{-}PCy_2)_2(NMe_2)_4$ (**2b**) (30 °C in toluene-d_8).

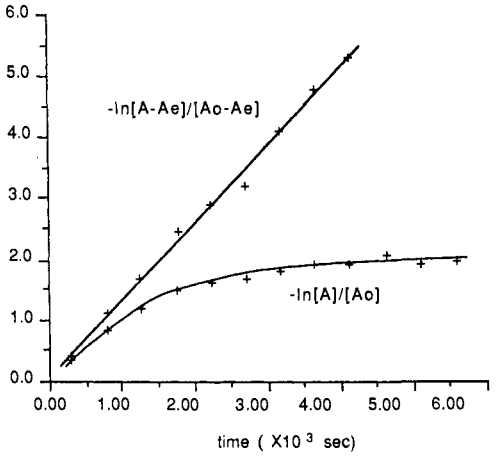

Figure 6. A plot of $-\ln [A - A_e]/[A_0A_e]$ vs time demonstrating the reversible first-order isomerization of $W_2(PPh_2)_2(NMe_2)_4$ (**5**) contrasted with the nonlinear plot of $-\ln [A]/[A_0]$ (40 °C in toluene-d_8).

the equilibrium favors the unbridged isomer by ca. 4:1 at ambient temperature. This suggests that the bis(di-*tert*-butylphosphido) complex may not form a bridged complex because of steric factors. On the other hand, the lack of bridge formation when R = $SiMe_3$

Table V. Barriers to Rotation, $\Delta G^*(T_c)$ (kcal/(mol K)), about M–N and M–P Bonds in $1,2\text{-}M_2X_2(NMe_2)_4$ and Related Complexes

M	X		M–NMe_2	M–N′Me_2	M–P(*t*-Bu)$_2$
Mo	NMe_2		11.5 ± 0.2 (243)[a]	N/A	N/A
W	NMe_2		11.2 ± 0.2 (238)[b]	N/A	N/A
Mo	cl		14.1[c]	N/A	N/A
W	Cl		13.9[c]	N/A	N/A
Mo	P(*t*-Bu)$_2$		8.2 ± 0.1 (185)[d]	11.5 ± 0.1 (260)	8.6 ± 0.1 (190)
Mo	P(*t*-Bu)$_2$		7.1 ± 0.2 (165)	N/A	
W	P(*t*-Bu)$_2$	(**1g**)	7.5 ± 0.1 (170)[d]	11.3 ± 0.1 (256)	9.7 ± 0.1 (212)
W	P(*t*-Bu)$_2$	(**1a**)	7.3 ± 0.2 (170)	N/A	
	PCy_2	(**2g**)			9.9 ± 0.5 (218)
	PCy_2	(**2a**)	9.0 ± 1.0 (204)		
	PEt_2	(**3a**)	9.8 ± 0.2 (224)	N/A	
	$P(SiMe_3)_2$	(**4a**)	11.5 ± 0.1 (263)	N/A	8.4 ± 0.2 (175)
	PPh_2	(**5a**)	12.0 ± 0.1 (273)	N/A	
	P(*p*-tol)$_2$	(**6g**)	10.6 ± 0.3 (240)	11.1 ± 0.2 (250)	
	P(*p*-tol)$_2$	(**6a**)	12.0 ± 0.1 (273)	N/A	
	P(*p*-FPh)$_2$	(**7g**)	9.4 ± 0.5 (208)	12.9 ± 0.3 (293)	
	P(*p*-FPh)$_2$	(**7a**)	12.1 ± 0.1 (273)	N/A	
	$Cl/P(SiMe_3)_2$	(**9a**)	10.5 ± 0.1 (237)	16.1 ± 0.1 (348)	
	$P(t\text{-}Bu)_2/PPh_2$	(**13a**)	8.8 ± 0.1 (198)	11.7 ± 0.1 (268)	
	$P(SiMe_3)_2/PCy_2$	(**14a**)	9.6 ± 0.1 (219)	11.6 ± 0.1 (263)	
	$1,1\text{-}W_2Cl(P(t\text{-}Bu)_2)(NMe_2)_4$	(**18**)			16.2 ± 0.2 (344)

[a] Chisholm, M. H.; Cotton, F. A.; Frenz, B. A.; Reichert, W. W.; Shive, L. W.; Stults, B. R. *J. Am. Chem. Soc.* **1976**, *98*, 4469. [b] Chisholm, M. H.; Cotton, F. A.; Extine, M. W.; Stults, B. R. *J. Am. Chem. Soc.* **1976**, *98*, 4477. [c] Akiyama, M.; Chisholm, M. H.; Cotton, F. A.; Extine, M. W.; Murillo, C. A. *Inorg. Chem.* **1977**, *16*, 2407. [d] Buhro, W. E.; Chisholm, M. H.; Folting, K.; Huffman, J. C. *J. Am. Chem. Soc.* **1987**, *109*, 905.

Table VI. Energetic Parameters for Anti–Gauche Isomerization in 1,2-$M_2(PR_2)_2(NMe_2)_4$ (ΔG and ΔH Values in kcal/mol and ΔS Values in eu)

parameter	M = Mo, R = *t*-Bu	M = W, R = *t*-Bu	M = W, R = Ph
$\Delta H°$	−0.3 ± 0.2	−0.5 ± 0.4	+2.8 ± 0.5
$\Delta S°$	−1.5 ± 0.5	−0.3 ± 1.1	+4.2 ± 1.5
$\Delta G°$(298 K)	+0.1 ± 0.1	−0.4 ± 0.1	+1.5 ± 0.1
ΔH_f^*	+17.9 ± 0.4	+18.8 ± 0.6	
ΔS_f^*	−13.8 ± 1.1	−10.6 ± 1.9	
ΔG_f^*(298 K)	+22.1 ± 0.1	+22.0 ± 0.1	
ΔH_r^*	+18.3 ± 0.4	+19.4 ± 0.6	
ΔS_r^*	−12.2 ± 1.2	−10.1 ± 2.0	
ΔG_r^*(298 K)	+22.0 ± 0.1	+22.4 ± 0.1	

Table VII. Barriers for Wing Flapping of the Phosphido Bridges, $\Delta G^*(T_c)$ (kcal/(mol K)), Obtained from α-Cyclohexyl Protons of PCy_2 and $OC(CH_3)_3$ Resonances in Toluene-d_8 Solutions

complex		NMe_2	α-Cy	O-*t*-Bu
$W_2(\mu\text{-}PCy_2)_2(NMe_2)_4$	**2b**	12.3 (240)	12.1 (252)	
$W_2(\mu\text{-}PPh_2)_2(NMe_2)_4$	**5b**	10.1 (208)		
$W_2(\mu\text{-}P(p\text{-tol})_2)_2(NMe_2)_4$	**6b**	10.3 (210)		
$W_2(\mu\text{-}P(p\text{-FPh})_2)_2(NMe_2)_4$	**7b**	10.4 (210)		
$W_2(\mu\text{-}PCy_2)_2(O\text{-}t\text{-}Bu)_4$	**19b**		12.8 (264)	13.0 (261)
$W_2(\mu\text{-}PPh_2)_2(O\text{-}t\text{-}Bu)_4$				8.4

Table VIII. Temperature Dependence of the ^{31}P NMR Chemical Shifts (ppm) and $^1J_{PW}$ (Hz) in Parentheses for 1,2-$W_2(PR_2)_2(NMe_2)_4$ Complexes

complex	room temp	−40 °C	−80 °C	Δδ
1g, R = *t*-Bu	201.4 (335)	194.0 (328)	191.5 (327)	9.9 (8)[b]
2g, R = Cy	157.0 (348)	153.5 (344)	151.7 (342)	5.25 (6)[a]
		152.9 (338)	149.0 (331)	–[b]
5a, R = Ph	61.6 (204)	55.0 (194)	51.6 (186)	10.0 (18)[b]
5g, R = Ph	85.2 (253)	76.6 (234)	71.2 (215)	14.0 (38)[b]
8g, Cl/R = *t*-Bu	169.0 (224)	162.2 (222)	156.5 (213)	12.5 (11)[b]
9a, Cl/R = $SiMe_3$	−100.3 (228)		−105.7 (225)	5.4 (3)[a]
	−100.1 (225)	−106.7 (226)	−110.3 (223)	10.2 (2)[b]

[a] $C_6D_5CD_3$. [b] THF.

may be due to both steric and electronic factors. For the aryl-phosphido complexes, electronic factors are important in establishing an equilibrium between the bridged and unbridged isomers since the PPh_2 ligand is less sterically demanding than the PCy_2 ligand.

Thermodynamic and activation parameters for phosphido-bridge formation are given in Table IX. A number of points are worthy of mention. (1) The activation parameters for phosphido-bridge formation are similar to those for anti ⇄ gauche isomerization. Thus the two processes may have common features, namely a decogging of proximal substitution across the M–M bond after which M–M rotation or bridge formation is rapid. (2) It cannot be determined whether or not bridge formation occurs from anti or gauche rotamers since anti ⇄ gauche isomerization is faster than bridge closure. (3) The entropy of activation which is very small for the bisphosphido compound **5** becomes large and negative for the compound $W_2(PPh_2)(P(t\text{-}Bu)_2)(NMe_2)_4$. Thus although the latter compound undergoes irreversible bridge formation it does so very slowly. It therefore remains possible that a bridged isomer of $W_2(P(t\text{-}Bu)_2)_2(NMe_2)_4$ is thermodynamically favored but kinetically inaccessible from the unbridged isomer. (4) In no instance have we observed a monobridged species. The closing (and opening) of bridges must occur in a cooperative manner as is often seen in transition-metal carbonyl chemistry.[10]

(e) A Comparison of Amido and Phosphido Ligands. This work affords an excellent opportunity to compare the ligating properties of amido and phosphido ligands. Both are capable of acting as π donors and the following question arises: Which is the better π donor? The same question is commonly asked of alkoxide and thiolate ligands, often without a clear resolution because of opposing effects in orbital energetics and metal–ligand bond distances. Here, in the unbridged isomers 1,2-$W_2(PR_2)_2(NMe_2)_4$ there are two orbitals at each metal center (the $d_{x^2-y^2}$ and d_{xy} when the M–M axis is defined as the *z* axis) that are empty and available to receive π-electron density. There are three filled ligand p_π orbitals at each metal center so there must be one lone pair which is ligand centered. In the parent compounds $M_2(NMe_2)_6$ this lone pair is delocalized over the NMe_2 ligands. However, in the present cases there is good evidence that it is localized on phosphorus. This can be seen from the pyramidal coordination at phosphorus and also by a consideration of the M–N/P distances. In the compounds $Mo(NMe_2)_4$ and $Mo(PCy_2)_4$, which because of symmetry and electron counting have four metal–ligand double bonds, the parameter Δ (defined as the difference between M–P and M–N distances) is 0.34 Å. In the five cases reported here the value of Δ is in the range 0.42–0.50 Å (Table III).

Of particular note with regard to M–P π bonding is the beautiful work of Baker et al.[11] and the remarkable structure of the $Cp_2Hf(PEt_2)_2$ molecule. Here there is only one vacant metal π-acceptor orbital for two phosphorus lone pairs. One lone pair is evidently used in π bonding and the other is not, giving rise to one short Hf–P distance, 2.488 (1) Å, and one long Hf–P distance, 2.682 (1) Å, involving trigonal-planar and pyramidal coordination at phosphorus, respectively. This difference in Hf–P distances, 0.2 Å, may be taken as a difference between a single and a double bond. In our work we find that the W–P distances are close to those expected for single bond distances. Note that the W–P distances in the bridged isomers are essentially the same length as those in the unbridged isomers and in the latter they must be single bonds.

There is, of course, a problem in looking only to structural parameters deduced from crystallography. (1) The changes in distances and angles are relatively small. (2) The structural data provide information only about the ground-state properties of the molecule in the solid state. There is evidence from solution studies that PR_2 ligands are involved in some degree of π bonding to these W_2^{6+} centers as is outlined below.

First, if we look to the barriers of M–NMe_2 rotation in 1,2-$M_2X_2(NMe_2)_4$ compounds we generally find that electronegative and poor π-donating ligands X yield high barriers, greater than the value 12 kcal mol^{-1} found for X = NMe_2. In the case of the mixed phosphido–amido compounds (X = PR_2) we find fairly low barriers indicating the *overall* strong electron releasing properties ($\sigma^2 + \pi^2$) of the phosphido ligand. There is too a marked dependence on R such that the electron releasing order for PR_2 would be estimated at R = *t*-Bu > Cy > $SiMe_3$ > aryl. See Table V. Also in the gauche rotamers there are two barriers to M–N bond rotation because there are two types of NMe_2 ligands. These barriers generally bracket those of the anti rotamer. We have also measured the barriers to M–P bond rotation in a number of instances. These are not dissimilar from those associated with M–N bond rotations. This contrasts with M–C rotational barriers in compounds of formula 1,2-$M_2(Ar)_2(NMe_2)_4$.[12] In the latter the aryl ligands are bladed in the same manner as the NMe_2 ligands and thus have proximal and distal ortho hydrogens (groups). However, rotations about the M–C bonds are evidently too fast to be frozen out on the NMR time scale at −90 °C indicating barriers to rotation about M–C bonds must be less than ca. 7 kcal mol^{-1}.

Of course in the compounds of formula 1,2-$W_2(PR_2)_2(NMe_2)_4$ it is not clear that we can ignore steric factors completely. However, our claim that electronic factors are most important does seem reasonable and is reinforced by a consideration of the rotational barriers in the mixed phosphido compounds of formula

(10) Cotton, F. A.; Wilkinson, G. In *Advanced Inorganic Chemistry*, 5th ed.; Wiley and Sons: New York, 1988; p 1325.

(11) Baker, R. T.; Whitney, J. F.; Wreford, S. S. *Organometallics* **1983**, *2*, 1049.

(12) Chetcuti, M. J.; Chisholm, M. H.; Folting, K.; Haitko, D. A.; Huffman, J. C.; Janos, J. *J. Am. Chem. Soc.* **1983**, *105*, 1163.

Table IX. Ground-State and Activation Parameters for the Formation of Phosphido Bridges in $W_2(PR_2)_2(NMe_2)_4$ Complexes (ΔG and ΔH Values in kcal/mol, ΔS Values in eu, and Free Energies (G) Calculated at 313 K Unless Stated Otherwise)

	a R = Cy	b R = Ph	c R = *p*-tol	d R = *p*-FPh	e R = *t*-Bu, R′ = Cy	f R = *t*-Bu, R′ = Ph
$\Delta G°$		−1.0	−1.7 (312 K)	−1.2 (312 K)	0.8 (295 K)	
$\Delta H°$		1.5 ± 0.8				
$\Delta S°$		8.1 ± 2.4				
			Unbridged → Bridged			
$\Delta G^{\ddagger}$	22.7	22.6	22.3	22.3		24.9
$\Delta H^{\ddagger}$	18.8 ± 0.5	22.5 ± 0.8				18.5 ± 0.3
$\Delta S^{\ddagger}$	−12.4 ± 2.0	−0.3 ± 2.9				−20.6 ± 0.8
			Bridged → Unbridged			
$\Delta G^{\ddagger}$		23.7	24.0	23.5		
$\Delta H^{\ddagger}$		20.9 ± 1.3				
$\Delta S^{\ddagger}$		−8.9 ± 2.7				

1,2-$W_2(PR_2)(PR'_2)(NMe_2)_4$. Moreover in the compound 1,1-$W_2Cl(P(t\text{-}Bu)_2)(NMe_2)_4$ the barrier to M–P bond rotation (16.2 (2) kcal/mol) is essentially double that of the 1,2-isomer, consistent with the view than when only one NMe_2 ligand is present at the tungsten center then the PR_2 ligand is called upon to act as a full $\sigma^2 + \pi^2$ donor.

The second probe of the extent of M–P π bonding comes from ^{31}P NMR studies. It is generally agreed that the distribution of electron density in the σ bonds between phosphorus and its substituents, the extent to which phosphorus participates in π bonding, and the variations in the coordination geometry at phosphorus are major contributors to the observed chemical shifts.[7] One-bond coupling constants can normally be understood within the framework of the Fermi contact term. Thus, for a given atom, Z, variations in PZ coupling appear to be dominated by variation of the s-electron density brought about by changes in hybridization at phosphorus.

In general, characterization of the phosphido ligand, PR_2^-, has focused on the more common phosphido-bridged structures, because data on terminal phosphido ligands are more scarce. However, the recent observation by Baker et al.[11] that the resonances for the singly and doubly bonded PCy_2 ligands, in the frozen out ^{31}P NMR spectrum of $Cp_2Hf(PCy_2)_2$, resonate at −15.3 and 270.2 ppm, respectively (a chemical shift difference of 285 ppm), suggests that the ^{31}P chemical shifts may be quite sensitive probes for evaluating the degree of M–P multiple bonding in a complex.

The series of complexes *anti*-1,2-$W_2(P(t\text{-}Bu)_2)_2(NMe_2)_4$ (**1a**), *gauche*-1,2-$W_2(P(t\text{-}Bu)_2)_2(NMe_2)_4$ (**1g**), and 1,1-$W_2Cl(P(t\text{-}Bu)_2)(NMe_2)_4$ (**18**) reveals a progressive downfield shift from 178.2 to 257.7 ppm. Similarly the $^1J_{PW}$ coupling constant increased from 287 to 412 Hz on going from **1a** to **18**. Having kept constant the substituents at phosphorus, the oxidation state of the metal, and the gross structural features of the complexes, the variation in the observed chemical shifts and coupling constants can most reasonably be attributed to a change in the W–P interaction. The low-field chemical shift and increase in the P–W coupling constant can be understood from the increase in s character as the terminal phosphido ligand is rehybridized sp^3 to sp^2 upon W–P multiple-bond formation. Loss of s character from the phosphorus lone pair has a deshielding effect on the nucleus, yielding a low-field chemical shift.[7] Increased s character in the W–P bond, with the sp^2-hybridized phosphorus, results in an increased tungsten–phosphorus coupling constant. A similar correlation between a very-low-field chemical shift and a large value of $^1J_{^{183}W-^{31}P}$ was previously observed by Malisch and coworkers[13] for the complexes $CpW(CO)_2(PR_2)$ where R = *t*-Bu and *i*-Pr.

In order to extend the relationship of the metal–phosphorus bonding and the respective ^{31}P chemical shifts to complexes with different substituents at phosphorus, the substituent effects on the free secondary phosphines must be considered. The secondary phosphines corresponding to the phosphido ligands of complexes **1–7** resonate between 20.1 and −237.4 ppm as shown in Table X. The abnormally-high-field resonance for $HP(SiMe_3)_2$ has been attributed to a phosphorus lone pair of high s character.[7] Calculation of the parameter $\Delta\delta$ (eq 5), which represents the down-field shift of the coordinated phosphide resonance from the parent secondary phosphine, provides a comparison of the relative strength of the tungsten–phosphorus interactions (see Table X). Coincident with the increase in the parameter $\Delta\delta$ is an increase in the magnitude of the phosphorus–tungsten coupling constant from 204 Hz in **4a** to 411 Hz for **18**. A plot of $J_{^{183}W-^{31}P}$ versus $\Delta\delta$ is shown in Figure 7.

$$\Delta\delta = \delta(\text{phosphide}) - \delta(\text{phosphine}) \quad (5)$$

Table X. Comparison of ^{31}P NMR Data for Secondary Phosphines and Mixed Amido–Phosphido Complexes

phosphine	δ, ppm ($^1J_{PH}$, Hz)	complex	δ, ppm ($^1J_{PW}$, Hz)	$\Delta\delta$, ppm
$HP(t\text{-}Bu)_2$	20.1 (187)[a]	**1a**	178.2 (285)	158.1
		1g	199.7 (333)	179.6
$HPCy_2$	−27.5 (195)[a]	**2a**	133.7 (312)	161.2
		2g	156.5 (341)	184.0
$HPEt_2$	−55.5 (190)[b]	**3a**	70.7 (230)	126.2
		3g	91.1 (270)	146.6
$H(PSiMe_3)_2$	−237.4[c]	**4a**	−106.7 (244)	130.7
		4g	−89.3 (246)	148.1
$HPPh_2$	−40.1 (214)[a]	**5a**	61.8 (207)	101.9
		5g	88.4 (262)	128.5
$HP(p\text{-}tol)_2$	−42.1 (214)[a]	**6a**	63.3 (214)	105.5
		6g	91.3 (282)	133.4
$HP(p\text{-}FPh)_2$	−43.7 (217)[a]	**7a**	57.4 (204)	101.1
		7g	79.4 (256)	123.1

[a] In C_6D_6 solution, measured at 146.2 MHz. [b] Moedritzer, K.; Maier, L.; Groenweghe, L. C. D. *J. Chem. Eng. Data* **1962**, *7*, 307. [c] Fluck, E.; Heckmann, G. In *Phosphorus-31 NMR Spectroscopy in Stereochemical Analysis*; Verkade, J. G., Quin, L. D., Eds.; VCH Publishers: Deerfield Beach, FL, 1987; p 61.

The PZ coupling constants of coordinated phosphines, ZPR_3, are known to vary as a function of the other substituents at phosphorus. The variation in the proton–phosphorus coupling constants of the parent secondary phosphines, HPR_2 (Table X), shows the expected increase with increasing electronegativity of the other substituents at phosphorus.[14] However, coordination of the phosphido ligand to tungsten shows exactly the opposite substituent effect on the phosphorus–tungsten coupling constant. The observed phosphorus–tungsten coupling constant increases with increasing basicity of the respective secondary phosphines and is consistent with a decrease in the "lone pair effect" upon M–P multiple-bond formation. The term "lone pair effect" has been used by Verkade and Quinn to describe the tendency for s-electron density to reside within a lone pair as observed from the $^1J_{^{31}P-^1H}$ values of PH_4^+ (546–548 Hz), PH_3 (182–195 Hz),

(13) Jörg, K.; Malisch, W.; Reich, W.; Meyer, A.; Schubert, U. *Angew. Chem., Int. Ed. Engl.* **1986**, *25*, 92.

(14) Augmented s character in the P–Z bond caused by increased electronegativity of the remaining phosphorus substituents is expected to increase the magnitude of the P–Z coupling constant in the absence of the countervailing lone pair effect.

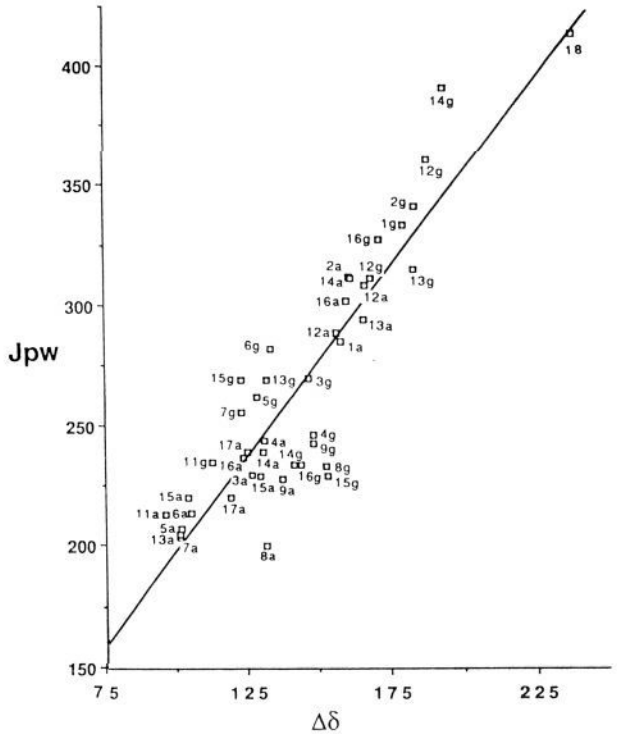

Figure 7. Plot of the parameter $\Delta\delta$ (ppm) vs $^1J_{PW}$ (Hz) for complexes **1–18**.

and PH_2^- (138–140 Hz). The s character residing in a lone pair has a shielding effect on the phosphorus nucleus. Upon multiple bond formation, s character is transferred out of the lone pair and into the P–Z bond such that in the double bond limit the lone pair is a pure p orbital.

The chemical shifts and tungsten–phosphorus coupling constants of all the mixed amido–phosphido complexes examined by variable-temperature ^{31}P NMR spectroscopy show a significant temperature dependence. On lowering the temperature from room temperature to −80 °C a high-field chemical shift ($\Delta\delta$ = 7.6–13.9 ppm), as well as a 2–38 Hz decrease in the $^1J_{PW}$, was observed (see Table VIII).

In addition, a temperature-dependent coalescence of apparently a single chemical shift (Figure 4) is observed for *gauche*-1,2-$W_2(PCy_2)_2(NMe_2)_4$ (T_c = −30 °C), *anti*-1,2-$W_2(PCy_2)(P(SiMe_3)_2)(NMe_2)_4$ (T_c = <−80 °C), and *gauche*-1,2-$W_2Cl(P(SiMe_3)_2)(NMe_2)_4$ (T_c = −80 °C). This dynamic process can most reasonably be accounted for by freezing out (on the NMR time scale) the inversion of the phosphido ligand in a pyramidal conformation as observed in the solid-state structures. The observed coalescence behavior may be due to the equilibrium between various invertamers with only one invertamer being present in a significant concentration at the low-temperature limit.[9]

Such a freezing of the phosphido ligands into pyramidal configurations at low temperature is consistent with the observed high-field shift of the ^{31}P resonances and decrease in the phosphorus–tungsten coupling constant at low temperature. The low-field shift and increased phosphorus–tungsten coupling constant at higher temperatures are consistent with a time-averaged increase in the metal–phosphorus bonding. Or alternately expressed, at low temperature there is less M–P π bonding and the phosphorus is more pyramidal.

In conclusion there is good evidence from the NMR studies that the PR_2 ligands are π donating to some extent in solution and that chemical shifts, coupling constants, and M–P rotational barriers are informative with respect to the degree of this M–P π bonding.

(f) A Comparison of the Bonding in Bridged and Unbridged Isomers. The bonding in the ethane-like dimers is understood from earlier studies.[2] Each metal forms three metal–ligand σ bonds, two metal–ligand π bonds, and a metal-to-metal triple bond

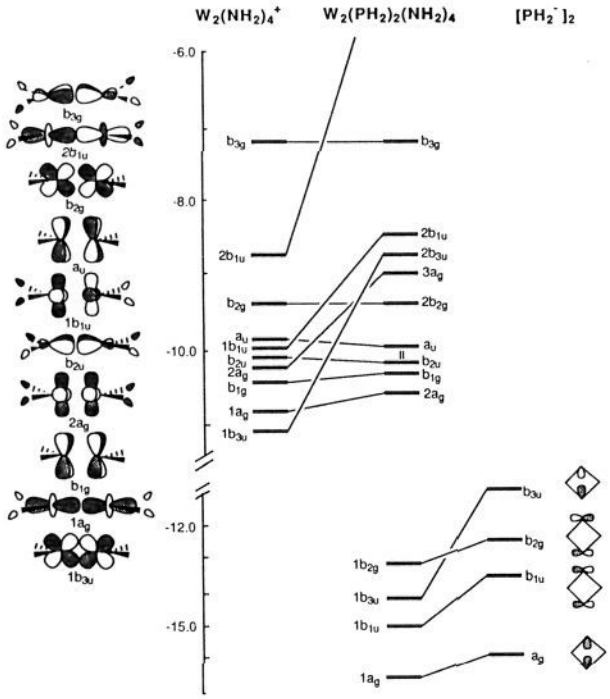

Figure 8. An interaction diagram describing the construction of an idealized D_{2h} phosphido-bridged dimer $W_2(\mu\text{-}PH_2)_2(NH_2)_4$ from the $W_2(NH_2)_4^{2+}$ and $[PH_2^-]_2$ fragments. Note that the metal- and phosphorus-fragment orbitals are plotted on different energy scales. The b_{2u} molecular orbital is the HOMO.

comprising one σ and two π components. In a bitetrahedron of the type shown below it is primarily the e_g metal d orbitals that are available for M–M bonding and as shown this will give rise to σ and δ interactions. See II below. This d^3–d^3 interaction is

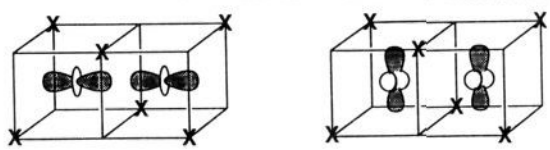

II

expected to give a MO configuration of $\sigma^2\delta^2\delta^{*2}$. *This, of course,* ignores mixing of M–M and M–L bonding, but this simple description does serve to point out that the bitetrahedron favors metal–ligand bonding (each metal forms four M–L bonds) at the expense of M–M bonding and furthermore that upon bridge formation the M–M bond order changes from 3 to 1.

Since the $\Delta H°$ values are small in the cases where we find an equilibrium involving bridged and unbridged isomers we can say, to a first approximation, that the formation of two additional W–P bonds is roughly equivalent to the loss of two W–W π bonds. Of course, there is also a change in M–M σ bonding since the M–M distances differ by nearly 0.3 Å in the bridged and unbridged structures.

A more detailed bonding description in these phosphido-bridged d^3–d^3 dimers was obtained from a fragment molecular orbital analysis[15] on the model complex $W_2(\mu\text{-}PH_2)_2(NH_2)_4$. The influence of the phosphido bridges on the M–M bonding was examined by the construction of an idealized D_{2h} structure (planar $W_2(\mu\text{-}P)_2$ core as in an edge-shared bitetrahedron) from $W_2(NH_2)_4^{2+}$ and two $[PH_2^-]$ fragments. This was then allowed to distort to the observed structure with a puckered W_2P_2 core and inequivalent amide ligands.

A simplified interaction diagram of $W_2(NH_2)_4^{2+}$ and $[PH_2^-]_2$ fragments is presented in Figure 8. The metal-based orbitals,

(15) Summerville, R. H.; Hoffmann, R. H. *J. Am. Chem. Soc.* **1976**, *98*, 7240.

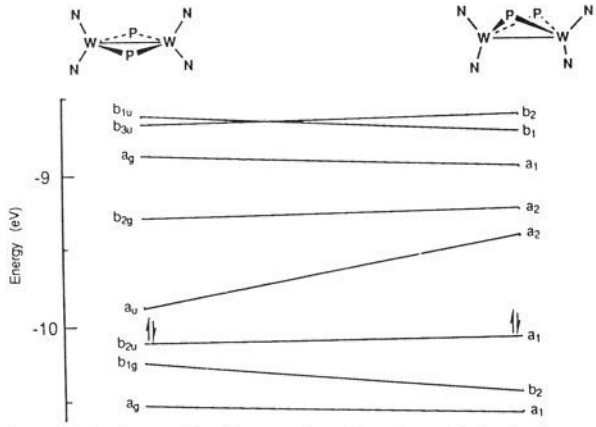

Figure 9. An interaction diagram describing the variation in the metal-based orbitals of $W_2(\mu\text{-}PH_2)_2(NH_2)_4$ on distortion from a planar D_{2h} to a puckered C_{2v} geometry.

shown at the left-hand side of the figure, represent the combination of two ML_2 fragments. The z^2 and xz metal–ligand nonbonding orbitals of the ML_2 fragment form metal–metal σ and π bonding and antibonding combinations ($1a_g$, $1b_{3u}$, b_{2g}, and $2b_{1u}$, respectively). The in-phase and out-of-phase combinations of the δ-type xy orbitals, b_{1g} and a_u, are destabilized by π donation from the amido lone pairs. The x^2-y^2 orbitals form weak δ-type interactions, $2a_g$ and $1b_{1u}$. The yz orbitals (metal–ligand antibonding) also form metal–metal π bonding and antibonding interactions (b_{2u} and b_{3g}). This set of M–M orbitals for the hypothetical fragment $W_2(NH_2)_4^{2+}$ is occupied by six electrons.

The above metal-based orbitals are destabilized upon interaction with the phosphido lone pair orbitals a_g and b_{3u}, which are perpendicular to the W_2N_4 plane, as well as with the b_{1u} and b_{2g}, which are parallel to the metal–metal vector. The metal π-type $1b_{3u}$ and δ-type $2a_g$ orbitals, as well as the higher lying $1b_{1u}$ and b_{2g} orbitals, interact strongly with the phosphido ligand set leaving a $\sigma^2\pi^2\delta^2$ metal–metal bonding configuration with a very small δ to δ^* HOMO/LUMO gap. Though frequently overshadowed by the π-donor ability of terminal-phosphido ligands, the P–H σ^* orbitals of the phosphido bridges, not pictured on this diagram, are capable of accepting π-electron density from the metals, analogous to the π-acceptor characteristics of PR_3 ligands. This weak interaction causes a minor stabilization of the b_{1g} orbital and may contribute to the shorter M–P bonds in the bridged complex **2b** than in the unbridged **2g**.

Distortion from an idealized D_{2h} structure to the puckered geometry observed in the crystal structure of **2b** results in both an increase in the metal–metal bonding and an increase in the HOMO–LUMO gap as shown in Figure 9. The major driving force for the observed distortion is localized within the b_{1g} δ-bonding orbital, which, upon distortion to C_{2v} symmetry, is of the same symmetry as the higher π-type b_{3u} (both the b_{1g} and b_{3u} orbitals have b_2 symmetry in the C_{2v} point group). The mixing of these orbitals results in a hybridization of the occupied-metal-based orbital in favor of metal–metal bonding, but away from the phosphido ligands in order to minimize M–P antibonding in occupied orbitals as shown in III (D_{2h}) and IV (C_{2v}) below. The

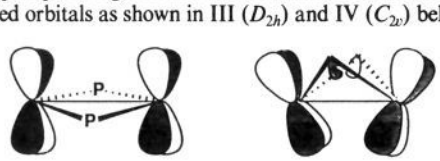

III

IV

maximization of the metal–metal bonding at the expense of some metal–phosphorus interaction by the puckered distortion is also reflected by the increase of the metal–metal overlap population (0.575 vs 0.635 for D_{2h} and C_{2v}, respectively) and decrease in the metal–phosphorus overlap population (0.724 vs 0.648 for D_{2h} and C_{2v}, respectively). The destabilization of the LUMO on distortion to the puckered geometry, shown in V (D_{2h}) and VI (C_{2v}) below,

V VI

mirrors the stabilization of the b_2 orbital. The δ^*, a_u and π^*, b_{2g} orbitals (both a_2 symmetry in the C_{2v} point group), although they are directed toward the bridges, are hybridized so as to minimize both metal–metal and metal–phosphorus antibonding. The destabilization of this hybridized metal orbital, which happens to be the LUMO, reflects the reorganization of the metal–phosphorus and metal–metal bonding in the puckered structure.

The total metal–NH_2 interaction is approximately constant and independent of the W_2P_2 distortion. However, a slight preference for bonding to the amido ligand in the equatorial site of the puckered structure is observed from the total W–N Mulliken overlap populations ($N_a = 0.546$, $N_e = 0.595$, where N_e and N_a are defined in drawing I).

The preference for the puckered geometry observed for the $W_2(PR_2)_2(NMe_2)_4$ complexes is clearly driven by a maximization of metal–metal bonding at the expense of some metal–phosphorus interaction. However, the barrier to inversion of the phosphido bridges, "wing-flapping", by which the puckered structure passes through a planar transition state is quite low, consistent with experimental measurements (see Table VII). Further examination of the interaction diagram (Figure 9) suggests that while the d^3–d^3 phosphido-bridged tetrahedral dimers, $W_2(\mu\text{-}PR_2)_2(NR'_2)_4$, exhibit a preference for a puckered structure, the formal reduction to a d^4–d^4 phosphido-bridged tetrahedral dimer should exhibit a preference for a planar geometry. It is difficult, however, to generalize the geometric preference of phosphido-bridged tetrahedral dimers, $M_2(\mu\text{-}PR_2)_2X_4$, based on the d-electron count for d^1–d^1, d^2–d^2, and d^3–d^3 dimers because the relative energies of particularly the b_{2u} and b_{1u} orbitals are largely influenced by the attendant ligands, X.

Concluding Remarks. The synthesis and characterization of compounds of formula $W_2(PR_2)_2(NMe_2)_4$ has allowed us to examine a number of interesting aspects of bonding. (1) In the unbridged ethane-like dimers the amido ligands are seen to be better π donors than the PR_2 ligands. However, in solution there is good evidence for the strong electron-releasing properties of the PR_2 ligands (R = *t*-Bu > Cy > $SiMe_3$ > Ar), and ^{31}P chemical shifts and ^{183}W–^{31}P coupling constants together with M–N and M–P rotational barriers provide a measure of phosphido $\sigma^2 + \pi^2$ donation. (2) In the bridged isomers, tungsten–phosphorus bonding is maximized but at the expense of metal–metal bonding. That in certain instances there exist equilibria involving bridged and unbridged isomers reveals the near thermochemical neutrality of the internally compensated system. (3) The puckered W_2P_2 moiety in the bridged isomers is a result of enhancing M–M bonding. (4) The opening and closing of phosphido bridges occurs in a cooperative manner. We have not seen any mono-phosphido-bridged species.

Finally it is worth noting the M–M distances in the d^4–d^4 phosphido-bridged dimers $Mo_2(\mu\text{-}P(t\text{-}Bu)_2)_2(P(t\text{-}Bu)_2)_2$ and $W_2(\mu\text{-}PCy_2)_3(PCy_2)_2^-$ are 2.209 (1)[16] and 2.550 (1) Å,[17] respectively. In the hypothetical reaction $M_2(\mu\text{-}PR_2)_2(PR_2)_2 + PR_2^- \rightarrow M_2(\mu\text{-}PR_2)_3(PR_2)_2^-$, the formation of the new metal–ligand bridge bond is made at the expense of M–M π bonding in a similar way to that seen in the work reported here.

Experimental Section

General Procedures. All manipulations were carried out in an inert atmosphere of dry and oxygen-free nitrogen using standard Schlenk and drybox techniques. Solvents were dried and distilled from sodium ben-

(16) Jones, R. A.; Lasch, J. G.; Norman, N. C.; Whittlesey, B. R.; Bright, T. C. *J. Am. Chem. Soc.* **1983**, *105*, 6184.
(17) Baker, R. J.; Krusic, P. J.; Tulip, T. H.; Calabrese, J. C.; Wreford, S. A. *J. Am. Chem. Soc.* **1983**, *105*, 6763.

zophenone ketyl and stored under nitrogen over 4 Å molecular sieves. Starting materials 1,2-$W_2Cl_2(NMe_2)_4$,[6] $LiP(t\text{-}Bu)_2$, $LiPCy_2$, $LiPEt_2$, $LiPPh_2$, $LiP(p\text{-tol})_2$, $LiP(p\text{-}C_6H_4F)_2$,[18] and $LiP(SiMe_3)_2(1.5THF)$[19] were prepared by literature procedures.

NMR spectra were recorded from benzene-d_6 and toluene-d_8 solutions. The ^1H NMR spectra were recorded on either a Nicolet NT-360 (361.07 MHz) or a Varian XL-300 (299.94 MHz) spectrometer. These spectra were calibrated against the residual protio impurities in the benzene-d_6 and toluene-d_8 solvents set at 7.15 and 2.09 ppm, respectively. The ^{31}P NMR spectra were recorded on a Nicolet NT-360 spectrometer (146.18 MHz). These spectra were calibrated against an 85% H_3PO_4 external standard set at 0.0 ppm. IR spectra were obtained from KBr pellets using a Perkin-Elmer 283 spectrometer. Elemental analyses were performed by Schwarzkopf Microanalytical Laboratory, Woodside, NY, and Oneida Research Services Inc., Whitesboro, NY.

1,2-$W_2(PR_2)_2(NMe_2)_4$ Compounds. The ditungsten–bisphosphido–tetraamido complexes were prepared by the reaction of 2 equiv of a lithium organophosphide salt in tetrahydrofuran (THF) at or below 0 °C, as described in detail for 1,2-$W_2(P(t\text{-}Bu)_2)_2(NMe_2)_4$. The ^1H and ^{31}P NMR data are given in Table I.

1,2-$W_2(P(t\text{-}Bu)_2)_2(NMe_2)_4$ (1). A magnetically stirred solution of 1,2-$W_2Cl_2(NMe_2)_4$ (0.750 g, 1.22 mmol) in THF (15 mL) was cooled to −40 °C with a CH_3CN/liquid N_2 slush bath. To this a solution of $LiP(t\text{-}Bu)_2$ (0.380 g, 2.5 mmol) in THF (10 mL) was added dropwise via cannula. The resulting red-orange mixture was stirred an additional 30 min at −40 °C. The cold bath was removed and the reaction mixture was stirred for 1 h at room temperature. The solvent was evaporated in vacuo to give an orange residue which was extracted from LiCl with 20 mL followed by 10 mL of hexane. The combined extracts were filtered through Celite and then reduced in volume to about 5 mL and stored at −25 °C. The rotamers **1g** and **1a** were codeposited as large red-orange crystals and a yellow powder, respectively. These were collected by filtration and dried in vacuo (0.611 g, 0.732 mmol, 60%). Red-orange **1g** and yellow **1a** were separated manually, and both achieved equilibrium gauche:anti (**1g**:**1a**) ratios of 3.9:1.0 within a few hours in solution at room temperature. Orange crystals of **1a** were obtained from a toluene solution of **1** that was stored 5–6 weeks at −25 °C. Anal. Calcd for $C_{24}H_{60}N_4P_2W_2$: C, 34.55; H, 7.25. Found: C, 34.86; H, 7.48. IR data for **1g** (cm^{-1}): 2978 m, 2958 m, 2940 m, 2852 s, 2808 s, 2763 s, 1472 m, 1463 m, 1458 m, 1428 w, 1422 w, 1392 w, 1382 m, 1353 m, 1239 m, 1164 m, 1141 m, 1123 m, 1040 m, 1020 w, 953 s, 941 s, 792 m, 558 m, 350 w, 322 w.

1,2-$W_2(PCy_2)_2(NMe_2)_4$ (2). **2** was prepared according to the procedure described for **1** above, with the exception that the reaction temperature was never allowed to exceed 0 °C. The crude reaction mixture was extracted at 0 °C with toluene from which a crystalline product **2g** was isolated in an 80% yield. Isolated **2g** achieved a gauche:anti (**2g**:**2a**) equilibrium ratio of 5:1 within 1.5 h at 7 °C. At room temperature **2** readily rearranges to $W_2(\mu\text{-}PCy_2)_2(NMe_2)_4$ ($t_{1/2}$ ca. 1 h). Anal. Calcd for $C_{32}H_{68}N_4P_2W_2$: C, 40.95; H, 7.30. Found: C, 41.00; H, 7.33. IR data for **2g** (cm^{-1}): 2920 s, 2851 s, 2815 m, 2765 m, 1445 m, 1415 w, 1383 w, 1246 m, 1188 w, 1145 w, 1123 w, 1045 w, 1023 w, 997 w, 955 s, 883 w, 848 w, 719 w, 550 w.

1,2-$W_2(PEt_2)_2(NMe_2)_4$ (3). A stirred solution of 1,2-$W_2Cl_2(NMe_2)_4$ (0.300 g, 0.489 mmol) in Et_2O (15 mL) was cooled to −78 °C with a dry ice/acetone bath. To this, a solution of $LiPEt_2$ (0.94 g, 0.98 mmol) in Et_2O (5 mL) was added dropwise via cannula. The solution was left to stir at −78 °C for 2 h. As the reaction proceeded, the color of the reaction mixture changed from yellow to orange-brown and a bright orange precipitate of **3a** formed. The reaction mixture was filtered and the precipitate was collected on a glass frit. The product was dried in vacuo at 0 °C (0.210 g, 0.291 mmol, 59%). **3a** is thermally sensitive and can be handled at room temperature for periods of less than 1 h. In solution at 0 °C a gauche:anti (**3a**:**3g**) equilibrium ratio of 3.1:1 is established within 20 min. Also, at 0 °C, **3** isomerizes to its bridged isomer $W_2(\mu\text{-}PR_2)_2(NMe_2)_4$ ($t_{1/2}$ ca. 1 h). Above 0 °C all three isomers (anti, gauche, and bridged) decompose.

1,2-$W_2(P(SiMe_3)_2)_2(NMe_2)_4$ (4). **4** was prepared according to the procedure described for **1** above. The crude reaction mixture was extracted with hexane. The hexane solution of **4** was left to stand at room temperature overnight. Rotamer **4a** was deposited as a yellow crystalline product in a 30–50% yield. In solution, at room temperature, **4** exists almost exclusively as the anti rotamer. Anal. Calcd for $C_{20}H_{60}Si_4N_4P_2W_2$: C, 26.72; H, 6.74; N, 6.23. Found: C, 26.64; H, 6.44; N, 6.04. IR data for **4a** (cm^{-1}): 2938 m, 2850 s, 2810 m, 2758 m, 1610 w, 1438 m, 1415 w, 1392 w, 1379 w, 1236 s, 1140 m, 1117 w, 1036 w, 951 s, 938 s, 836 s, 754 w, 737 w, 676 w, 622 m, 556 w, 465 m, 438 m, 339 w.

1,2-$W_2(PPh_2)_2(NMe_2)_4$ (5). **5** was prepared according to the procedure described for **2** above with 0.300 g of 1,2-$W_2Cl_2(NMe_2)_4$ in THF (10 mL) and 0.190 g of $LiPPh_2$ in THF (10 mL). Under more concentrated reaction conditions competitive formation of $[Li][W_2(PPh_2)_3(NMe_2)_4(THF)_x]$[20] is observed. The crude reaction mixture of **5** was extracted with toluene at 0 °C from which a microcrystalline yellow product, **5a**, was isolated in a 60% yield. Isolated **5a** achieved a gauche:anti (**5g**:**5a**) equilibrium ratio of 1:6.6 within 10 min at room temperature. However, **5** readily rearranged to $W_2(\mu\text{-}PPh_2)_2(NMe_2)_4$ under these conditions ($t_{1/2}$ ca. 1.5 h). Anal. Calcd for $C_{32}H_{44}N_4P_2W_2$: C, 42.03; H, 4.86; N, 6.13. Found: C, 41.50; H, 4.60; N, 6.01.

1,2-$W_2(P(p\text{-tol})_2)_2(NMe_2)_4$ (6). **6** was prepared according to the procedure described for **2** above. Yellow microcrystalline **6a** was isolated from toluene solutions in a 50% yield. Isolated **6a** achieved a gauche:anti (**6g**:**6a**) equilibrium ratio of 1:3.8 within less than 5 min at 40 °C. Under these conditions **6** readily rearranged to $W_2(\mu\text{-}P(p\text{-tol})_2)_2(NMe_2)_4$ ($t_{1/2}$ ca. 1 h). Anal. Calcd for $C_{36}H_{52}N_4P_2W_2$: C, 44.55; H, 5.41; N, 5.77. Found: C, 44.18; H, 5.27; N, 5.45. IR data for **6a** (cm^{-1}): 3000 w, 2846 s, 2810 s, 2757 m, 1588 w, 1486 m, 1436 m, 1412 w, 1388 w, 1238 m, 1177 w, 1136 w, 1117 w, 1073 w, 1034 m, 1014 w, 941 s, 934 s, 795 s, 607 w, 545 w.

1,2-$W_2(P(p\text{-}C_6H_4F)_2)_2(NMe_2)_4$ (7). **7** was prepared according to the procedure described for **2** above. However, since $LiP(p\text{-}C_6H_4F)_2$ polymerized THF at room temperature, the reaction was carried out at −78 °C. It should be noted that $LiP(C_6H_4F)_2$ is thermally unstable with respect to decomposition and thus should be prepared from LiBu and the secondary phosphine immediately prior to use. Yellow microcrystalline **7a** was isolated from toluene solutions in a 15–20% yield. Isolated **7a** achieved a gauche:anti (**7g**:**7a**) equilibrium ratio of 1:2.6 in less than 5 min at 40 °C. Under these conditions **7** readily rearranged to $W_2(\mu\text{-}P(p\text{-}C_6H_4F)_2)_2(NMe_2)_4$ (**7b**) ($t_{1/2}$ ca. 1 h).

1,2-$W_2Cl(PR_2)(NMe_2)_4$ Compounds. Monophosphido-substituted complexes have been prepared by the controlled addition of 1 equiv of a lithium organophosphide to 1,2-$W_2Cl_2(NMe_2)_4$ in THF solutions.

1,2-$W_2Cl(P(t\text{-}Bu)_2)(NMe_2)_4$ (8). A stirred solution of 1,2-$W_2Cl_2(NMe_2)_4$ (0.500 g, 0.814 mmol) in THF (10 mL) was cooled to −78 °C. To this solution $LiP(t\text{-}Bu)_2$ (0.126 g, 0.830 mmol) in THF (6 mL) was added dropwise via cannula. The resulting orange solution was stirred an additional 40 min at −78 °C and then the cold bath was removed. After the mixture was allowed to warm for 15 min, the solvent was evaporated in vacuo. The resulting orange oil was extracted with two 10-mL aliquots of hexane and filtered through Celite. The filtrate contained **8**, 90% pure by NMR, with a gauche:anti equilibrium ratio of approximately 8:1 at room temperature. It was not possible to crystallize **8** from hexane, Et_2O, DME, pyridine, or CH_3CN.

1,2-$W_2Cl(P(SiMe_3)_2)(NMe_2)_4$ (9). A stirred solution of 1,2-$W_2Cl_2(NMe_2)_4$ (0.500 g, 0.814 mmol) in THF (10 mL) was cooled to −40 °C. To this, a solution of $LiP(SiMe_3)_2 \cdot 1.5THF$ (0.235 g, 0.803 mmol) in THF (10 mL) was added dropwise via cannula. The reaction mixture was stirred at −40 °C for 2 h and the solution turned a yellow-brown color. The reaction mixture was warmed to room temperature for an additional 30 min and then the volatiles were removed in vacuo. The yellow-brown residue was extracted with two 10-mL aliquots of hexane and filtered through Celite. The filtrate was reduced in volume to approximately 1 mL and within 1 h, on standing at room temperature, a yellow crystalline product, **9a**, was deposited (0.28 g, 0.37 mmol, 46%). Isolated **9a** achieved a gauche:anti (**9g**:**9a**) equilibrium concentration of about 1:3 within 1 h at room temperature. Anal. Calcd for $C_{14}H_{42}N_4Si_2W_2ClP$: C, 22.21; H, 5.60; N, 7.40. Found: C, 22.40; H, 5.35; N, 7.49. IR data for **9a** (cm^{-1}): 2930 m, 2856 s, 2812 m, 2766 m, 1596 m, 1458 m, 1439 m, 1418 m, 1381 w, 1240 s, 1142 m, 1120 w, 1036 m, 1018 m, 951 s, 938 s, 827 s, 742 m, 676 m, 621 m, 556 w, 467 w, 437 w, 360 w.

1,2-$W_2Cl(PCy_2)(NMe_2)_4$ (10). **10g** has only been observed by ^{31}P NMR as a minor product (<30%) in NMR tube reactions of 1,2-$W_2Cl_2(NMe_2)_4$ (30 mg, 0.0489 mmol) in THF (0.5 mL) with $LiPCy_2$ (8 mg, 0.039 mmol) at −80 °C. **2g** is the major product of this reaction.

1,2-$W_2Cl(PPh_2)(NMe_2)_4$ (11). Like **10**, **11** has only been observed by ^{31}P NMR spectroscopy in NMR tube reactions between 1,2-$W_2Cl_2(NMe_2)_4$ (30 mg, 0.049 mmol) and $LiPPh_2$ (9 mg, 0.46 mmol) in THF at −80 °C. A product distribution of 85% **5g**, 3% **5a**, 10% **11g**, and 2% **11a** was observed. The existence of **11** was confirmed by the addition of $LiP(t\text{-}Bu)_2$ (10 mg, 0.065 mmol) in THF (0.25 mL), after which the mixed phosphido product **13** was observed.

1,2-$W_2(PR_2)(PR'_2)(NMe_2)_4$ Compounds. Mixed phosphido complexes were prepared from the respective monophosphide monochloro complexes

(18) (a) Bartlett, R. A.; Olmstead, M. M.; Power, P. P. *Inorg. Chem.* **1986**, *25*, 1243. (b) Issleib, K.; Tzschach, A. *Chem. Ber.* **1959**, *92*, 1118.

(19) Fritz, G.; Hölderich, W. *Z. Anorg. Allg. Chem.* **1976**, *422*, 104.

(20) Chisholm, M. H.; Martin, J. D. Manuscript in preparation.

and 1 equiv of a second $LiPR_2$ reagent.

1,2-W_2($P(t\text{-Bu})_2$)(PCy_2)(NMe_2)$_4$ (12). Complex **8** was generated from 1,2-$W_2Cl_2(NMe_2)_4$ (0.500 g, 0.814 mmol) and $LiP(t\text{-Bu})_2$ (0.124 g, 0.816 mol) as described above. The crude reaction mixture was then recooled to −78 °C and a solution o f $LiPCy_2$ (0.166 g, 0.813 mmol) in THF (5 mL) was added dropwise to the orange solution. The reaction mixture was stirred an additional 15 min at −78 °C. The reaction vessel was transferred to a 0 °C bath and volatile components were removed in vacuo. The residue was extracted at 0 °C with hexane (2 × 5 mL) and filtered through Celite. The filtrate was reduced in volume to 5 mL. After standing at room temperature for 1.5 h the solution was briefly shock cooled in N_2(l) and then stored at −25 °C. Rotamer **12a** was deposited as yellow-orange crystals (0.224 g, 0.253 mmol, 31%). Isolated **12a** achieved a gauche:anti (**12g**:**12a**) equilibrium ratio of about 1:1 within a few hours at ambient temperature. Anal. Calcd for $C_{28}H_{64}N_4P_2W_2$: C, 37.94; H, 7.28. Found: C, 36.98; H, 7.25. IR data for **12a** (cm^{-1}): 2928 s, 2851 s, 2814 m, 2770 m, 1447 m, 1385 m, 1357 w, 1243 m, 1168 w, 1143 w, 1123 w, 1039 w, 955 s, 944 s, 887 w, 849 w, 815 w, 553 w, 420 w.

1,2-W_2($P(t\text{-Bu})_2$)(PPh_2)(NMe_2)$_4$ (13). **13** was prepared from the reaction between **8** and $LiPPh_2$ according to the procedure described for **12** above. Orange crystalline and yellow microcrystalline **13a** was isolated from hexane and toluene solutions, respectively, in a 42% yield. Isolated **13a** achieved a gauche:anti (**13g**:**13a**) equilibrium ratio of 1:1 within an hour at room temperature. Only at elevated temperatures, >40 °C, is the rate of isomerization to the bisphosphido-bridged isomer significant ($t_{1/2}$ = 24 h at 40 °C).

1,2-W_2($P(SiMe_3)_2$)(PCy_2)(NMe_2)$_4$ (14). A stirred solution of **9** (0.300 g, 0.396 mmol) in THF (10 mL) was cooled to −40 °C. To this was added a solution of $LiPCy_2$ (0.085 g, 0.417 mmol) in THF (5 mL). The reaction mixture was stirred at −40 °C for an additional 1 h and then warmed to 0 °C. After the mixture was stirred for 30 min at 0 °C the volatile components were removed in vacuo. The crude reaction mixture was extracted with hexane (10 + 5 mL) and filtered through Celite. The filtrate was reduced in volume to about 1 mL and yellow crystals of **14a**, suitable for an X-ray diffraction study, began to form immediately at room temperature (0.170 g, 0.196 mmol, 49%). Isolated **14a** achieved a gauche:anti (**14g**:**14a**) equilibrium ratio of about 1:1 after several hours at room temperature.

1,2-W_2($P(SiMe_3)_2$)(PPh_2)(NMe_2)$_4$ (15). **15** was prepared according to the procedure described for **14** above. Yellow crystals of **15a** were isolated from hexane solutions stored at −20 °C in a 22% yield. Isolated **15a** achieved a gauche:anti (**15g**:**15a**) equilibrium ratio of 1:5 after several hours at room temperature.

1,2-W_2($P(SiMe_3)_2$)($P(t\text{-Bu})_2$)(NMe_2)$_4$ (16) and 1,2-W_2($P(SiMe_3)_2$)(PEt_2)(NMe_2)$_4$ (17). **16** and **17** were observed by ^{31}P NMR spectroscopy in NMR-tube reactions of *anti*-1,2-$W_2Cl(P(SiMe_3)_2)(NMe_2)_4$ (30 mg, 0.040 mmol) and 1 equiv of the respective $LiPR_2$ in THF (0.5 mL). The solids were added to an NMR tube which was then cooled to −78 °C. After the solvent was added, the samples were placed into a temperature-controlled NMR probe to monitor the product formation. **17a** was observed to form rapidly at −78 °C. At room temperature, resonances consistent with the gauche rotamer were observed with a gauche:anti equilibrium ratio of about 1:3. **16** was not observed to form until temperatures greater than −20 °C. At room temperature, a gauche:anti equilibrium ratio of about 1:1.1 was achieved.

1,1-W_2Cl($P(t\text{-Bu})_2$)(NMe_2)$_4$ (18). Complex **8** was generated from 1,2-$W_2Cl_2(NMe_2)_4$ (0.500 g, 0.814 mmol) and $LiP(t\text{-Bu})_2$ (0.126 g, 0.830 mmol) in THF (13 mL) at −78 °C as described above. The cold bath was removed, the solution was allowed to warm for 10 min, and then the volume was reduced in vacuo to about 6 mL. The orange homogeneous mixture was transferred to a 10-mm NMR tube and the tube was flame sealed. As the sample stood at room temperature the color gradually turned dark yellow. Periodic monitoring by $^{31}P\{^1H\}$ NMR spectroscopy revealed the slow disappearance of **8** and the appearance of **18**. After 11 days, the NMR tube was opened, the solution was evaporated in vacuo, and the residue was extracted with hexane (12 + 8 mL) and filtered through Celite. Crude **18** was obtained as an orange oil by evaporation of the filtrate in vacuo which was 82% pure by ^1H NMR spectroscopy. The predominant impurity was **8** (11%). Attempts to crystallize **18** have been unsuccessful.

$W_2(\mu\text{-}PR_2)_2(NMe_2)_4$ Compounds. The bridged isomers, $W_2(\mu\text{-}PR_2)_2(NMe_2)_4$ (R = Cy, Et, Ph, *p*-tol, *p*-C_6H_4F) and $W_2(\mu\text{-}PR_2)(\mu\text{-}PR'_2)(NMe_2)_4$ (R = *t*-Bu; R′ = Cy, Ph), are prepared either by the isomerization of isolated unbridged isomers or from the reaction of the appropriate lithium phosphide salts with 1,2-$W_2Cl_2(NMe_2)_4$ in THF above 0 °C, as described in detail for $W_2(\mu\text{-}PCy_2)_2(NMe_2)_4$.

1,2-$W_2(\mu\text{-}PCy_2)_2(NMe_2)_4$ (2; 2.0 g, 2.1 mmol) was dissolved in hexane (15 mL) and magnetically stirred at room temperature for 8 h. Volatile components were then removed in vacuo leaving pure, microcrystalline **2b**. A sample of **2b** was recrystallized from DME at −20 °C resulting in single crystals suitable for the X-ray structural analysis. Anal. Calcd for $C_{32}H_{68}N_4P_2W_2$: C, 40.95; H, 7.30. Found: C, 40.59; H, 7.34. IR data (KBr, cm^{-1}): 2930 s, 2855 s, 2808 m, 2764 m, 1449 m, 1414 w, 1387 w, 1044 w, 1033 w, 1028 w, 1004 w, 961 m, 955 m, 942 m, 936 m, 888 w, 850 w, 755 w br, 726 w, 522 br, 413 br.

Alternatively, 1,2-$W_2Cl_2(NMe_2)_4$ (0.500 g, 0.814 mmol) was dissolved in THF (15 mL) and cooled to −40 °C in a CH_3CN/N_2(l) slush bath. To this, a solution of $LiPCy_2$ (0.332 g, 1.63 mmol) in THF (10 mL) was added dropwise with stirring. The reaction mixture was allowed to gradually warm to 0 °C and was magnetically stirred for one additional hour. The reaction mixture was then stripped to dryness. The residue was extracted with three 10-mL aliquots of toluene and filtered through Celite to remove the LiCl. The filtrate was allowed to stand at room temperature overnight. The volume of the filtrate was reduced to about 1 mL and stored at −20 °C. **2b** was deposited as a brown powder which was collected by filtration and dried in vacuo (isolated yield 0.397 g, 0.423 mmol, 52%).

It should be noted that it was not possible to isolate isomerically pure samples of $W_2(\mu\text{-}PR_2)_2(NMe_2)_4$ (R = Ph, *p*-tol, *p*-C_6H_4F) and $W_2(\mu\text{-}P(t\text{-Bu})_2)(\mu\text{-}PCy_2)(NMe_2)_4$, which exist in solution as equilibrium mixtures of the unbridged and bridged isomers.

The $W_2(\mu\text{-}PEt_2)_2(NMe_2)_4$ complex, **3b**, is thermally unstable with respect to decomposition at room temperature. All the other phosphido-bridged complexes reported here are stable, with respect to decomposition, in hydrocarbon solutions for several days under inert atmosphere conditions at ambient temperatures.

$W_2(\mu\text{-}PCy_2)_2(O\text{-}t\text{-Bu})_4$ (19b). A magnetically stirred solution of $W_2(\mu\text{-}PCy_2)_2(NMe_2)_4$ (0.367 g, 0.391 mmol) was taken up in toluene (8 mL) and cooled to −24 °C in a CCl_4/dry ice bath. To this was added 4 equiv of *t*-BuOH/benzene azeotrope (0.372 mL, 4.2 M). The reaction mixture was stirred for an additional 20 min at −24 °C and then placed at room temperature where and the volatile components were removed in vacuo. The dark solids were redissolved in a minimum amount of hexane and stored at −20 °C. Black cubic crystals, obtained in three successive crops, were isolated by filtration and washed with hexane (0.324 g, 0.307 mmol, 79%). No crystals were suitable for an X-ray diffraction study. The mother liquor was found to contain small amounts of an impurity (^{31}P NMR of impurity: δ = 226.5 (s, $^1J_{PW}$ = 365 Hz and $^1J_{PW}$ = 333 Hz). ^1H NMR (room temperature, toluene-d_8): δ (OC(C-H_3)$_3$) 1.52 ppm (s, 36 H); δ (C_6H_{11} α-protons) 2.31 ppm (br s, 4 H). Other cyclohexyl resonances cannot be uniquely identified but are broad resonances between 1.3 and 2.4 ppm.

^{31}P NMR (room temperature, benzene-d_6): δ = 250.7 ppm (s, $^1J_{PW}$ = 311 Hz, satellite intensity 26%).

Variable-Temperature NMR Studies. The dynamic behavior of the 1,2-$W_2(PR_2)_2(NMe_2)_4$ complexes was examined by variable-temperature ^1H (299.94 or 361.07 MHz) and $^{31}P\{^1H\}$ (146.18 MHz) NMR spectroscopy in toluene-d_8 or THF. Coalescence temperatures were determined by varying the probe temperatures in increments of ≤5 deg in the vicinity of the coalescence points. Temperatures were calibrated with methanol or ethylene glycol standard curves. the separations, $\Delta\nu$ (Hz), of the resonances for the proximal and distal amido and phosphido ligands in the low-temperature limiting spectra are tabulated in the supplementary material. These data were used to calculate rate constants and activation parameters for the exchange processes according to equations

$$k = \pi(\Delta\nu)/\sqrt{2}$$

and

$$\Delta G^{\ddagger} = \left[-\ln \frac{kh}{T_c k'}\right](RT_c)$$

Equilibrium distributions of the gauche and anti rotamers were determined in 0.01–0.02 M toluene-d_8 solutions by integrations of proton resonances. The averages of several measurements, made after equilibrium had been reached, were used in the calculations. Ground-state parameters $\Delta H°$, $\Delta S°$, and $\Delta G°$ are recorded in Table VI and were obtained from plots of ln (K_{eq}/2) vs $1/T$ according to the equation

$$\ln (K_{eq}/2) = -(\Delta H°/RT + \Delta S°/R)$$

Note the factor 2 accounts for the statistical distribution of 2:1 for the gauche and anti rotamers.

The dynamic behavior of $W_2(PR_2)_2(NMe_2)_4$ (R = Cy, Ph, *p*-tol, *p*-C_6H_4F) and $W_2(\mu\text{-}PCy_2)_2(O\text{-}t\text{-Bu})_4$ in toluene-d_8 solutions was examined by ^1H NMR spectroscopy at 299.94 MHz. Coalescence temperatures were determined by varying the probe temperatures in increments ≤5 deg in the vicinity of the coalescence points. Temperatures were

Table XI. Equilibrium Constants and Rate Data for the First-Order Unbridged to Bridged Isomerization in $W_2(PR_2)_2(NMe_2)_4$ Complexes

trial	T, K	half-lives followed	K_{eq}	k_{obs}, s^{-1}	$k_{forward}$, s^{-1}	$k_{reverse}$, s^{-1}
			(a) 1,2-$W_2(PCy_2)_2(NMe_2)_4$ → $W_2(\mu\text{-}PCy_2)_2(NMe_2)_4$			
1	299	3.2	NA	$(2.05 \pm 0.03) \times 10^{-4}$	NA	NA
2	303	3.3	NA	$(3.27 \pm 0.31) \times 10^{-4}$	NA	NA
3	311	2.4	NA	$(5.75 \pm 0.06) \times 10^{-4}$	NA	NA
4	311	2.6	NA	$(7.74 \pm 0.13) \times 10^{-4}$	NA	NA
5	317	1.7	NA	$(1.36 \pm 0.06) \times 10^{-3}$	NA	NA
6	317	1.4	NA	$(1.51 \pm 0.17) \times 10^{-3}$	NA	NA
7	322	1.2	NA	$(2.12 \pm 0.23) \times 10^{-3}$	NA	NA
8	322	1.8	NA	$(2.11 \pm 0.11) \times 10^{-3}$	NA	NA
			(b) 1,2-$W_2(PPh_2)_2(NMe_2)_4$ ⇌ $W_2(\mu\text{-}PPh_2)_2(NMe_2)_4$			
1	295.3	3.5	4.62	$(1.40 \pm 0.02) \times 10^{-5}$	$(1.15 \pm 0.01) \times 10^{-4}$	$(2.50 \pm 0.03) \times 10^{-5}$
2	313.0	6.9	6.04	$(1.26 \pm 0.03) \times 10^{-3}$	$(1.08 \pm 0.03) \times 10^{-3}$	$(1.78 \pm 0.05) \times 10^{-4}$
3	322.0	11.5	5.33	$(3.98 \pm 0.24) \times 10^{-3}$	$(3.35 \pm 0.20) \times 10^{-3}$	$(6.29 \pm 0.38) \times 10^{-4}$
4	322.4	7.9	6.49	$(3.93 \pm 0.42) \times 10^{-3}$	$(3.41 \pm 0.42) \times 10^{-3}$	$(5.27 \pm 0.65) \times 10^{-4}$
5	326.1	6.3	5.76	$(5.12 \pm 0.15) \times 10^{-3}$	$(4.37 \pm 0.13) \times 10^{-3}$	$(7.58 \pm 0.22) \times 10^{-4}$
			(c) 1,2-$W_2(P(p\text{-}tol)_2)_2(NMe_2)_4$ ⇌ $W_2(\mu\text{-}P(p\text{-}tol)_2)_2(NMe_2)_4$			
1	311.9	5.9	15.7	$(1.71 \pm 0.04) \times 10^{-3}$	$(1.61 \pm 0.04) \times 10^{-3}$	$(1.03 \pm 0.03) \times 10^{-4}$
			(d) 1,2-$W_2(P(p\text{-}FPh)_2)_2(NMe_2)_4$ ⇌ $W_2(\mu\text{-}P(p\text{-}PhF)_2)_2(NMe_2)_4$			
1	311.6	4.8	6.49	$(2.13 \pm 0.07) \times 10^{-3}$	$(1.85 \pm 0.06) \times 10^{-3}$	$(2.77 \pm 0.09) \times 10^{-4}$
2	311.6	3.1	7.33	$(1.44 \pm 0.07) \times 10^{-3}$	$(1.27 \pm 0.07) \times 10^{-3}$	$(1.73 \pm 0.09) \times 10^{-4}$
			(e) 1,2-$W_2(P(t\text{-}Bu)_2)(PPh_2)(NMe_2)_4$ → $W_2(\mu\text{-}P(t\text{-}Bu)_2)(\mu\text{-}PPh_2)(NMe_2)_4$			
1	295	3.4	NA	$(4.00 \pm 0.14) \times 10^{-6}$	NA	NA
2	302	2.8	NA	$(8.14 \pm 0.31) \times 10^{-6}$	NA	NA
3	302	2.9	NA	$(8.18 \pm 0.31) \times 10^{-6}$	NA	NA
4	316	3.8	NA	$(3.36 \pm 0.25) \times 10^{-5}$	NA	NA
5	316	3.7	NA	$(3.48 \pm 0.18) \times 10^{-5}$	NA	NA

calibrated with MeOH standards. The separation of the exchanging resonances, $\Delta\nu$ (Hz), in the low-temperature limiting spectra are given in the thesis.[1b] Activation parameters were calculated as described above. The T_c values of the two types of amido ligands are somewhat obscured by the nearly simultaneous coalescence of one set of proximal and distal methyl protons. Thus, the $\Delta\nu$ for the two types of amido ligands must be inferred from the average signals of the frozen out degenerate exchange of the proximal and distal methyl resonances.

Kinetic Studies. Reaction rates were monitored by ^1H NMR spectroscopy using a Nicolet NT-360 spectrometer equipped with a standard automated kinetics software package (KINET). Samples were prepared by adding 7 to 15 mg of the respective 1,2-$W_2(PR_2)_2(NMe_2)_4$ complexes to an NMR tube in a dry box. NMR sample tubes were capped with septa and cooled to 0 °C. The tubes were charged with 0.50 mL of dry and deoxygenated toluene-d_8. Samples were stored at ≤0 °C until they were placed into a temperature-controlled (±1 deg) NMR probe. NMR probe temperatures were calibrated with external ethylene glycol.

Samples of the $W_2(PR_2)(PR'_2)(NMe_2)_4$ dimers were placed into extended NMR tubes. After the solvent was added, as described above, the samples were frozen with liquid N_2 and the NMR tubes were sealed under vacuum, with a torch. Isomerization of $W_2(P(t\text{-}Bu)_2)(PPh_2)(NMe_2)_4$, at other than room temperature, were carried out in NMR tubes submerged in temperature-controlled (±2 deg) water baths. Reactions were quenched at 0 °C for data collection by ^1H NMR spectroscopy. The higher reaction temperatures caused an increase in the rate of decomposition of **11** as seen by the appearance of the $HP(t\text{-}Bu)_2$ doublet at 0.17 ppm.

The relative concentrations of the anti, gauche, and bridged isomers were determined by comparison of the integrations of the amido methyl protons in **2**, the ortho proton resonances in **5**, **6**, and **7**, and the *t*-Bu proton resonances in **13**, normalized to 100%. A precise measurement of the relative concentration of the gauche rotamers (R = Ph, *p*-tol, *p*-C_6H_4F) was impossible when present as less than 5% of the reaction mixture because of the signal-to-noise ratio. At later reaction times the relative concentration of the gauche rotamer was estimated from the observed concentration of the more abundant anti rotamer and the known respective gauche:anti equilibrium constants.

Because the gauche:anti isomerization of the unbridged dimers is facile at temperatures below which phosphido-bridge closure is observed, it is not possible to determine whether phosphido-bridge closure occurs from the anti or gauche rotamer. Thus, the probability of phosphido-bridge closure from the respective anti and gauche rotamers was assumed to be equal. Treating the concentrations of the anti and gauche rotamers as the concentration of total unbridged dimer, [unbridged], the kinetic expression is simplified to irreversible (**2** and **13**) and reversible (**5**, **6**, and **7**) first-order kinetics.

By monitoring the disappearance of the unbridged isomers as a function of time, first-order k_{obs} values (see Table XI) were obtained from plots of ln [A]/[A_0] vs time and ln [A − A_e]/[A_0 − A_e] vs time (see eqs 6 and 7). [A] = the relative concentration of unbridged isomers at a

$$\ln [A]/[A_0] = k_{obs}t \quad \text{(irreversible)} \tag{6}$$

$$\ln [A - A_e]/[A_0 - A_e] = -k_{obs}t \quad \text{(reversible)} \tag{7}$$

given time, [A_e] = the relative equilibrium concentration of unbridged isomers and [A_0] = the initial relative concentration of unbridged isomers. Reported errors represent the standard deviations from a least-squares analysis.[21] Elementary rate constants k_f and k_r were calculated from eqs 8 and 9. The activation parameters (reported in Table XI)

$$k_r = k_{obs}/(K_{eq} + 1) \tag{8}$$

$$k_f = k_r K_{eq} \tag{9}$$

were obtained from eq 10. Ground-state parameters recorded in Table

$$\ln (k/T) = -(\Delta H^*/RT + \ln (k'/h) + \Delta S^*/R) \tag{10}$$

XI were obtained from plots of ln (K_{eq}) vs $1/T$ (see Table XI for data) according to eq 11.

$$\ln K_{eq} = (\Delta H°/RT + \Delta S°/R) \tag{11}$$

Computational Procedures. Coordinates for model compounds $W_2(\mu\text{-}PH_2)_2(NH_2)_4$ were taken from the X-ray crystal structures of $W_2(\mu\text{-}PCy_2)_2(NMe_2)_4$ and idealized to C_2 symmetry. A N–H bond length of 1.10 Å and a P–H distance of 1.40 Å were used. The systematic distortion of the idealized $W_2(\mu\text{-}PH_2)_2(NH_2)_4$ butterfly, C_{2v} symmetry, to an idealized D_{2h} structure was examined. Three possible orientations of the amido ligands were examined: (1) all NH_2 ligand planes parallel to the metal–metal vector, (2) all NH_2 ligand planes perpendicular to the metal–metal vector, and (3) axial NH_2 ligand planes perpendicular and equatorial NH_2 ligand planes parallel to the metal–metal vector. The interaction diagram shown was derived from orientation 2.

Molecular orbital calculations were performed using the method of Fenske and Hall.[22] Fragment molecular orbital calculations of the $W_2(NH_2)_4^{2+}$ and $(PH_2)_2^{2-}$ fragments were performed. Atomic basis functions were generated by a best fit to Herman-Skillman atomic calculations using the methods of Bursten, Jensen, and Fenske.[23] Contracted double-ζ representations were used for the W 5d AO's as well as the P 3p and N 2p AO's. Basis functions for the metal atoms were generated from a +1 oxidation state with valence W 6s and W 6p ex-

(21) Least-squares analyses were performed using the program PCLST obtained from Professor Joseph J. Gajewski, Indiana University.
(22) Hall, M. B.; Fenske, R. F. *Inorg. Chem.* **1972**, *11*, 768.
(23) Bursten, B. E.; Jensen, J. R.; Fenske, R. F. *J. Chem. Phys.* **1978**, *68*, 3320.

ponents fixed at 1.80. An exponent of 1.16 was used for the H 1s atomic orbital.

Single-Crystal X-ray Structural Determinations. General operating procedures and listings of programs have been described.[24] A summary of crystal data is given in Table II. Full details are provided in the supplementary materials.

Acknowledgment. We thank the National Science Foundation for support and Professors John Verkade and Odile Eisenstein for valuable discussion. We also note that the compound $W_2(\mu\text{-}PPh_2)_2(O\text{-}t\text{-}Bu)_4$ reported in this paper was first prepared by Professor Bryan Eichhorn (current address: Department of Chemistry, The University of Maryland, College Park, MD 20742).

Registry No. 1a, 137566-81-5; **1g**, 106651-38-1; **2a**, 137566-82-6; **2b**, 110303-35-0; **2g**, 116212-37-4; **3a**, 137467-40-4; **3b**, 137467-41-5; **3g**, 137566-74-6; **4a**, 137467-42-6; **4g**, 137566-75-7; **5a**, 137467-43-7; **5b**, 137467-44-8; **5g**, 137566-76-8; **6a**, 137467-45-9; **6b**, 137467-46-0; **6g**, 137566-77-9; **7a**, 137467-47-1; **7b**, 137467-48-2; **7g**, 137566-78-0; **8**, 137567-64-7; **8a**, 137467-49-3; **8g**, 137566-79-1; **9**, 137567-65-8; **9a**, 137467-31-3; **9g**, 137566-65-5; **10g**, 137467-32-4; **11a**, 137467-33-5; **11g**, 137566-66-6; **12a**, 137566-67-7; **12b**, 116301-30-5; **12g**, 137566-68-8; **13a**, 137566-69-9; **13b**, 116301-31-6; **13g**, 137566-70-2; **14a**, 137467-34-6; **14g**, 137566-71-3; **15a**, 137467-35-7; **15g**, 137566-72-4; **16a**, 137467-36-8; **16g**, 137566-73-5; **17a**, 137467-37-9; **17g**, 137567-66-9; **18**, 137495-96-6; **19b**, 137467-38-0; *anti*-1,2-$Mo_2(P(t\text{-}Bu)_2)_2(NMe_2)_4$, 106651-37-0; *gauche*-1,2-$Mo_2(P(t\text{-}Bu)_2)_2(NMe_2)_4$, 137566-80-4; 1,2-$W_2Cl_2(NMe_2)_4$, 63301-81-5; $W_2(\mu\text{-}PPh_2)_2(O\text{-}t\text{-}Bu)_4$, 110303-34-9; Mo, 7439-98-7; W, 7440-33-7; $W_2(\mu\text{-}PH_2)_2(NH_2)_4$, 137467-39-1.

Supplementary Material Available: Listings of h, k, l, F_o, and F_c values for $Mo_2(P(t\text{-}Bu)_2)_2(NMe_2)_4$, *anti*-$W_2(P(t\text{-}Bu)_2)_2(NMe_2)_4$, *gauche*-$W_2(P(t\text{-}Bu)_2)_2(NMe_2)_4$, $W_2(P(cyclohexyl)_2)_2(NMe_2)_4$, $W_2(P(SiMe_3)_2)_2(NMe_2)_4$, and $W_2(P(C_6H_{11})_2)(P(SiMe_3)_2)(NMe_2)_4$ (56 pages). Ordering information is given on any current masthead page.

(24) Chisholm, M. H.; Folting, K.; Huffman, J. C.; Kirkpatrick, C. C. *Inorg. Chem.* **1984**, *23*, 1021.

A Molecular Dynamics Study of the Stability of Chymotrypsin Acyl Enzymes

Guy W. Bemis, Gail Carlson-Golab, and John A. Katzenellenbogen*

Contribution from the Department of Chemistry, University of Illinois, 1209 West California Street, Urbana, Illinois 61801. *Received June 17, 1991*

Abstract: We have investigated the enantioselectivity observed in the deacylation rates of a β-substituted β-phenylpropionyl chymotrypsin acyl enzyme by molecular dynamics simulations. The ca. 60-fold difference in deacylation rates for the *R* and *S* esters ($k_d(S) = 0.17$ min^{-1}; $k_d(R) = 0.0029$ min^{-1}) is presumed to derive from less optimal stabilization of reactive intermediates in the case of the *R* enantiomer. Structures for both *R* and *S* acyl enzymes were constructed starting from the X-ray structure of chymotrypsin phenylethaneboronic acid complex. The ester carbonyl oxygen was placed in the oxyanion binding hole (backbone NH's from Gly-193 and Ser-195), and the phenyl group was placed in the hydrophobic cleft. Structures corresponding to acyl enzymes in which the β-substituent, an acetonyl chain, was engaged in hydrogen bonding with seven possible hydrogen bond donors near the active site were generated. Only three of these (Met-192 NH, Gly-216 NH, and Ser-218 OH) survived rigorous molecular mechanics minimization, and these three structures, in both the *R* and *S* acyl enzyme series, were subjected to molecular dynamics. In all three *R* acyl enzymes, the crucial hydrogen interaction between the ester carbonyl oxygen and the oxyanion binding hole was weakened during the dynamics run, whereas in two of the three *S* acyl enzymes, these hydrogen bonds persisted. There was also some rearrangement of the hydrogen-bonding configuration for the acetonyl side chain. An additional molecular dynamics study was done on the tetrahedral intermediates corresponding to the deacylation of the *R* and *S* acyl enzymes. Although, as expected, the hydrogen-bonding interaction between the oxyanion in the tetrahedral intermediate and the hydrogen bond donors in the oxyanion binding hole was strengthened for both enantiomers, the *R* enantiomer showed less ideal stabilization. These results provide a rationalization for the deacylation enantioselectivity of these acyl enzymes: The reduced deacylation rate of the *R* enantiomer could arise from less effective hydrogen-bonding stabilization of both the ester carbonyl in the acyl enzyme and the oxyanion in the deacylation tetrahedral intermediate by the oxyanion binding hole site; the *S* enantiomer, which preserves excellent hydrogen bond distances and geometry at both stages, is more ideally set up for the attack of water that leads to deacylation.

Introduction

The prodigious catalytic activity of serine proteases and their substrate specificity have long fascinated researchers. More recently, certain proteases of this class have become targets for the development of potent, selective inhibitors that might prove to have therapeutic utility.[1] A clearer understanding of the structural and stereochemical factors that control the stability of the various intermediates in the serine protease-catalyzed hydrolysis pathway would assist in the development of such inhibitors. Nevertheless, despite a clear general understanding of the specificity interactions[2] and major functional features involved in the hydrolysis process,[3] and despite many crystallographic studies on free proteases, as well as those complexed with both small and macromolecular complexes,[4] there has been little success in predicting how particular substrates and inhibitors will interact with protease active sites.

(1) For general references on the medical importance of protease inhibitors, see: (a) Rich, D. H. In *Comprehensive Medicinal Chemistry. The Rational Design, Mechanistic Study and Therapeutic Applications of Chemical Compounds*; Hansch, C., Sammes, P. G., Taylor, J. B., Eds.; Pergamon: New York, 1990. (b) *Design of Enzyme Inhibitors as Drugs*; Sandler, M., Smith, H. J., Eds.; Oxford University: Oxford, 1989. (c) *Proteases. Potential Role in Health and Disease*; Hörl, W. H., Heidland, E., Eds.; Plenum: New York, 1984.

(2) Segal, D. M.; Powers, J. C.; Cohen, G. H.; Davies, D. R.; Wilcox, P. E. *Biochemistry* **1971**, *10*, 3728-3738.

(3) Kraut, J. *Annu. Rev. Biochem.* **1977**, *46*, 311-358.

(4) These structures are available from the Brookhaven Protein Data Bank.

0002-7863/92/1514-570$03.00/0